Journal of MATERIALS RESEARCH

Invited Feature Paper-Review
DOI:10.1557/s43578-021-00443-8

ULTRA-WIDE BANDGAP MATERIALS, DEVICES, AND SYSTEMS

FOCUS ISSUE

Status of the growth and fabrication of AlGaN-based UV laser diodes for near and mid-UV wavelength

Ronny Kirste[1,2,a)], Biplab Sarkar[1,3], Pramod Reddy[1,2], Qiang Guo[1], Ramon Collazo[1], Zlatko Sitar[1]

[1] Department of Materials Science and Engineering, North Carolina State University, Raleigh, USA
[2] Adroit Materials, Cary, USA
[3] Department of Electronics and Communication Engineering, Indian Institute of Technology, Roorkee, Uttarakhand 247667, India
[a)] Address all correspondence to this author. e-mail: rkirste@ncsu.edu

Received: 17 June 2021; accepted: 15 November 2021; published online: 15 December 2021

In this article, the development of mid-UV laser diodes based on the AlGaN materials system is reviewed. The targeted wavelength for these lasers covers the range from 200 to 350 nm. After introducing UV laser diodes and explaining their applications, the challenges in growth, design, and fabrication are discussed. In addition, recent results from optically and electrically injected UV laser diodes are presented. Finally, we will discuss possible pathways to improve performance and give an outlook on the expected development of UV laser diodes in the near future.

Introduction

The first GaAs-based semiconductor laser diode was demonstrated in 1962, only two years after the realization of the first gas laser [1, 2]. Initially, operation of the devices was limited to low temperatures (77 K), needed high injection current densities, and relied on pulsed operation. After another decade of research and the invention of the double-heterojunction, separate-confinement structures by Alferov, GaAs lasers were able to provide continuous wave (cw) emission at room temperature in 1970 [3]. Today, almost all diode lasers emitting in the red and infrared wavelength range are based on the AlGaInAs system and have found broad applications and commercialization with a multibillion dollar optical communications market that secures millions of jobs worldwide. The extension into the visible wavelength range using arsenides is not possible due to the narrow bandgap of the material. Based on their stability, InGaN-based laser diodes emerged as the dominating technology for green to blue diodes. Using GaN and InGaN active regions, electrically injected lasing spanning the range from 360 nm up to the red wavelength region was demonstrated, and laser diodes with wavelengths down to 370 nm are commercially available [4, 5]. Nowadays, a further extension of the available laser diode spectrum is sought after, with focus on the UV range using AlGaN as the active region. While there are some successful attempts on the Ga-rich side with electrically injected lasing being demonstrated around 330 nm, shorter wavelengths are still challenging [6]. So far, only two groups succeeded in achieving electrically injected lasing in the UVC range [7, 8]. The challenges to achieve UV lasing from Al-rich AlGaN-based laser diodes with emission < 350 nm are manifold and include control of high-quality AlGaN growth, limited doping capabilities, low confinement and high loss in the laser cavities, high resistance contacts, and limited carrier injection capabilities. Only when all of these challenges are addresses simultaneously in one device, electrically injected UV lasing is possible.

This review article is giving an overview over the development of AlGaN-based UV laser diodes emitting in the sub-350 nm regime. Following this introduction, possible applications and the impact UV laser diodes may have in the future are presented. Growth of AlGaN layers and related challenges are presented next, with special focus on using different substrates and the reduction of point defects in the epitaxial layers. Doping challenges will be discussed and pathways to achieve high free electron and hole concentrations in Al-rich AlGaN will also be highlighted. While the design of UV laser diodes in general follows that of InGaN and AlGaAs-based devices, there are design challenges specific to the AlGaN-based system that will be summarized, including the p-GaN contact, waveguides and the refractive index, and design of the active region. Fabrication

and packaging of UV laser diodes will be addressed and results from electrically injected laser diodes present in literature will be highlighted. Finally, an outlook on possible future developments and pathways to improve UV lasing are included.

Applications, requirements, and economics of AlGaN-based UV laser diodes

Lasers emitting in the UV find broad applications in many fields ranging from lithography to quantum computing. The dominating technology for UV lasers are gas lasers, followed by frequency doubled visible or infrared lasers for some niche applications. For many applications, AlGaN-based laser diodes could replace these conventional emitters by providing coherent light emission in the UVA (350–315 nm), UVB (315–280 nm), or UVC (280–210 nm) range. The advantage of laser diodes over gas lasers is obvious: Laser diodes are significantly smaller, more robust against vibrations, need much simpler power supplies, have lower power consumption and higher efficiency, are potentially much cheaper if mass produced, similar to LEDs or VIS laser diodes, are more versatile allowing for portable applications, and have much longer lifetimes. The main downside of semiconductors compared to gas laser is their low beam quality. The prime materials system for the growth and fabrication of UV laser diodes is the AlGaN materials system (Fig. 1—left). This is based on its wide, direct bandgap and the proven capability to dope AlGaN over the whole compositional range to produce p/n junctions [9]. Laser diodes emitting at wavelength > 300 nm typically would be grown using Ga-rich AlGaN and devices emitting < 300 nm would be based on Al-rich AlGaN. Demonstration and commercialization of a sub 300 nm cw UV laser diode is understood as an enabling technology that will spawn many unexpected applications. Several potential applications

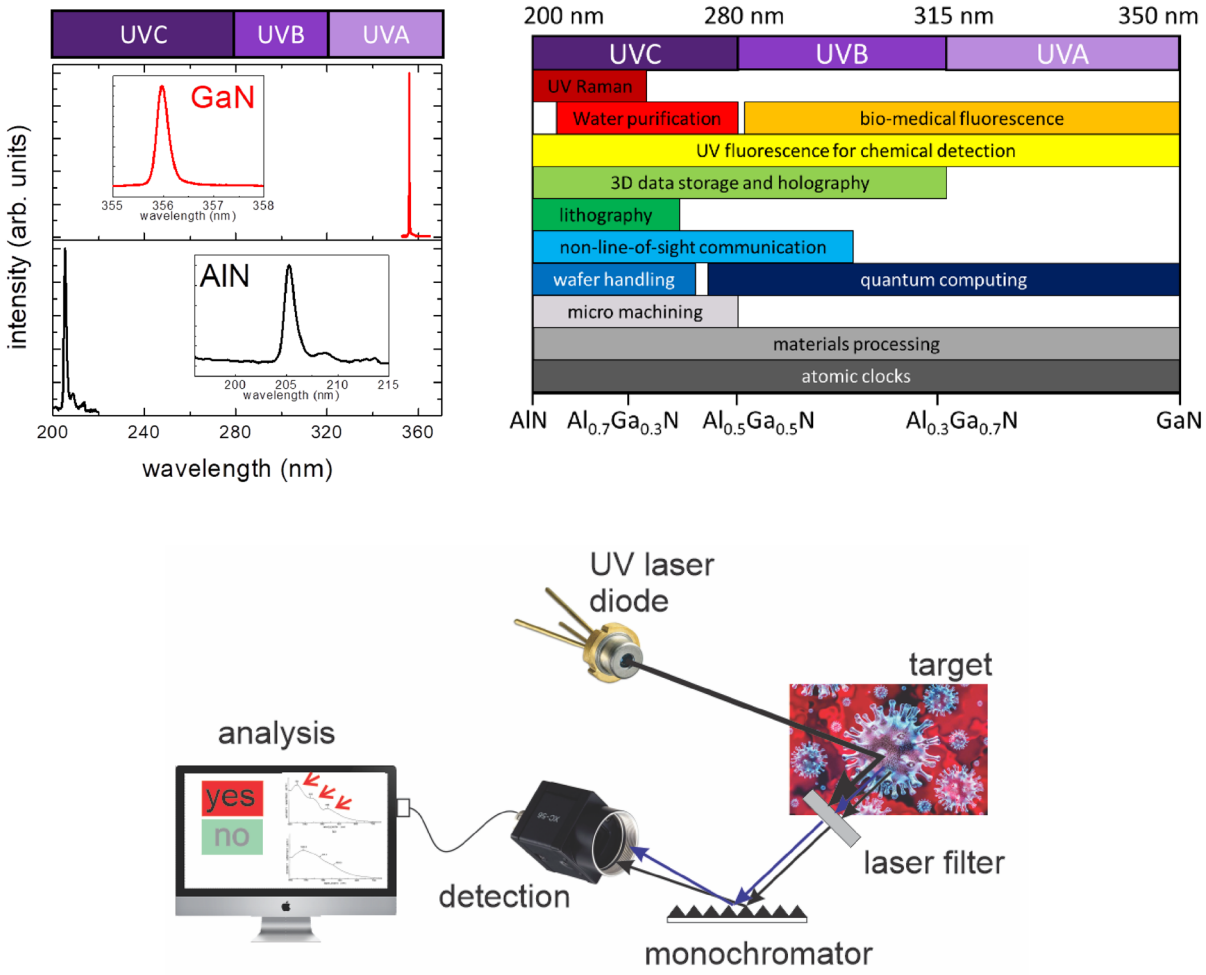

Figure 1: (left) Bandgap emission of GaN and AlN illustrating that the ternary semiconductor AlGaN can cover the UVA, UVB and UVC wavelength range. (right) Potential applications for AlGaN-based UVA (350–320 nm), UVB (315–280 nm), and UVC (280–200 nm) laser diodes. For most applications, gas lasers find already broad application, but laser diodes would, given they provide the desired power and beam quality, be superior for various reasons. (bottom) Schematic image for a UVC-based Raman spectroscopy system to detect viruses.

TABLE 1: Potential applications for UV diode laser.

Wavelength (nm)	Application	cw power (mW)	Comments
< 240	Excitation for portable UV Raman spectroscopy to identify bacteria, virus, chemical, fungi detection/ sensing [10–12]	≈ 100	Narrow linewidth needed (< 1 nm); cross section increases for lower wavelength; many chemicals have UV resonances; fluorescence interference is minimized with ultraviolet excitation below 260 nm
220–270	Water purification [13]	> 1000	Similar to UV LEDs; may circumvent challenges in light extraction efficiency in LEDs
280–350	Fluorescence spectroscopy for in-vivo bio-medical detection/tissue diagnostics [14, 15]	1–10	Absorption and resonance depend on tissue; low power needed to avoid damage; beam quality negligible
200–350	Fluorescence spectroscopy for chemical detection [16, 17]	> 100	Absorption (excitation) is specific to the molecule
< 320	UV high-density data storage [18] and holography [19]	< 10	Volumetric 3D, rather than a surface 2D, approach may be needed; high beam quality needed, price may be driving force
< 260	UV lithography [20]	> 1000	High power needed, replace excimer laser
< 300	non-line-of-sight communication [21, 22]	> 1000	Power determines range, good beam quality needed
< 270	Wafer singulation & laser lift-off [23]	> 10 k	High power density needed—pulsed lasing reasonable
> 280	Quantum computing with trapped ions [24, 25]	< 10	Wavelength depends on qubit, high beam quality needed, very narrow lines needed
< 280	Micro machining [26, 27]	> 1000	High power needed, pulsed, currently Nd:YAG (SHG)
< 350	Materials processing including drilling and separation [28, 29]	> 1000	High power, better resolution, UV allows for low temperature processing reducing damage, includes welding and curing
> 230	Excitation for atomic clocks [30, 31]	< 1	Similar to quantum computing, needs accurate control of wavelength and narrow laser line

have previously been identified and are summarized in Fig. 1 (right) and Table 1.

Figure 1 highlights several potential application fields for UV laser diodes. The potential applications are very diverse and include application as excitation sources for atomic clocks or qubits, for detection/sensing systems, and basic materials processing. In general, three main application fields can be identified: (1) materials processing and manipulation, (2) sensing/detection, and (3) others. Materials processing and manipulation is usually achieved using gas/solid state lasers but could be simplified or improved by using semiconductor lasers. This includes, e.g., lithography and curing, wafer singulation and lift-off, metal processing, low temperature drilling and separation, and to some extend micro machining. Many of these applications could benefit from AlGaN-based laser diodes by making processes more stable, more cost effective, or more flexible, while reducing damage due to high temperatures typically involved in IR laser machining. Furthermore, the reduced wavelength allows for better resolution and smaller working areas. While for many of these applications, the beam quality and line width are not important, those applications need high power densities, comparable to those achieved in the pulsed ArF and KrF lasers. The second set of applications are sensing applications and include resonant ultraviolet Raman spectroscopy and fluorescence spectroscopy and have been often demonstrated under laboratory conditions (Fig. 1—bottom). The advantage of both techniques is that they rely on resonances in the targeted materials, making the methods very sensitive, and provide high signal to noise ratio. Furthermore, these sensing applications would operate in the solar blind spectral range, which further reduces noise and increases efficiency. Optical spectra have been established for many materials and possible applications, such as detection of hazardous chemicals/bacteria/viruses, exposure of explosives, or monitoring of water quality, seems plausible. However, given the size and power consumption of the available UV laser sources, the desired mobile and rapid characterization, or continuous monitoring systems seem only possible if UV laser diodes are implemented. The laser wavelength for the spectroscopy applications depends on the targeted probe, with Raman applications being positioned rather in the UVC range, and fluorescence more in the UVB and UVA range. While power can be low (~ 10 mW cw to avoid damage of probed materials) these spectroscopy/sensing applications need a good beam quality and narrow lines in the range of 0.5 nm.

The applications in the third group are very diverse and span from quantum computing to water purification. Quantum computing, atomic clocks, and data storage are somewhat similar in terms that these applications are still very immature and need very well-defined laser beams. For example, for atomic clocks, the center wavelength needs to be accurate to at least four digits and the FWHM is desired to be < 0.01 nm to enable resonant excitation of the host atoms. The advantage

of laser diodes over gas lasers for these applications is the possibility of on-chip integration, which enables high device density and in combination with III/Nitride detectors, switches, and AlN waveguides a UV integrated optics system [32]. While achieving the needed technical specifications may be challenging initially, UV laser diodes will see an accelerated development harnessing experience from laser diodes emitting in the VIS and IR. Finally, other applications including non-line-of-sight communication and water purification require high power densities and are therefore rather further in the future.

The economic impact of the UV laser diodes cannot be underestimated. Considering that the laser diode market is expected to be as big as $6–7 billion in 2022, with the annual growth rates exceeding 5%, and that the UV LED market will be $1 billion in 2021, one can expect similar revenues for UV laser diodes. Therefore, UV laser diodes are not only important as an enabling technology but will also have a substantial economic impact.

AlGaN UV laser diode challenges

Figure 2 shows a schematic of an AlGaN-based UV laser diode. The main design of such diodes follows relatively closely that of InGaN and InGaAs laser diodes [33–35]. An active region with a multi quantum well (MQW) and electron blocking layer (EBL) is sandwiched between a p- and n-waveguide. A p- and n-cladding layer provide optical confinement. Contacts are made to the n-cladding layer and a hole-injection layer, typically a thin p-GaN film. Figure 2 also highlights the main challenges that come with this design, some of them being unique to UV laser diodes. The main challenge for all diodes, independent of the emission wavelength (IR/VIS/UV) and type (laser/LED) is always control of defects. This includes control of strain and dislocations in the epitaxial layers and control of point defects, including impurities and vacancies. Because of strong carrier localization, InGaN-based multiple quantum well (MQW) structures exhibit relatively high quantum efficiency even with threading dislocation densities (TDDs) of 1×10^9 cm^{-2} [36]. In contrast, optical and electronic properties of AlGaN and its MQW structures deteriorate rapidly at high TDDs [37]. Since threading dislocations act as current leakage paths, bulk GaN and AlN substrates with low TDDs are desired for fabrication of AlGaN-based LDs with long lifetimes. Indeed, the first electrically injected UVC laser diode and the best optically pumped laser diodes were all achieved on single crystalline substrates [8, 38]. The point defects (impurities, vacancies, complexes, etc.), on the other hand, need to be tightly controlled during growth [39–45] Thereby, the focus for UV laser diodes should be on point defects that either act as optical traps, reducing the IQE of the active region, or act as compensators limiting the doping capabilities [46]. This also includes losses on the p-side, related to p-doping, that contributes to the absorption loss in the waveguide [47, 48]. Accordingly, various defects have been identified in AlGaN, which may serve as sources of absorption losses and Shockley–Read–Hall recombination resulting in lower IQE [49, 50].

Other challenges that need to be addressed in order to improve electrically injected UV lasing are more specific to the targeted wavelength and AlGaN materials system. On the p-side, the main challenges are related to doping, contact

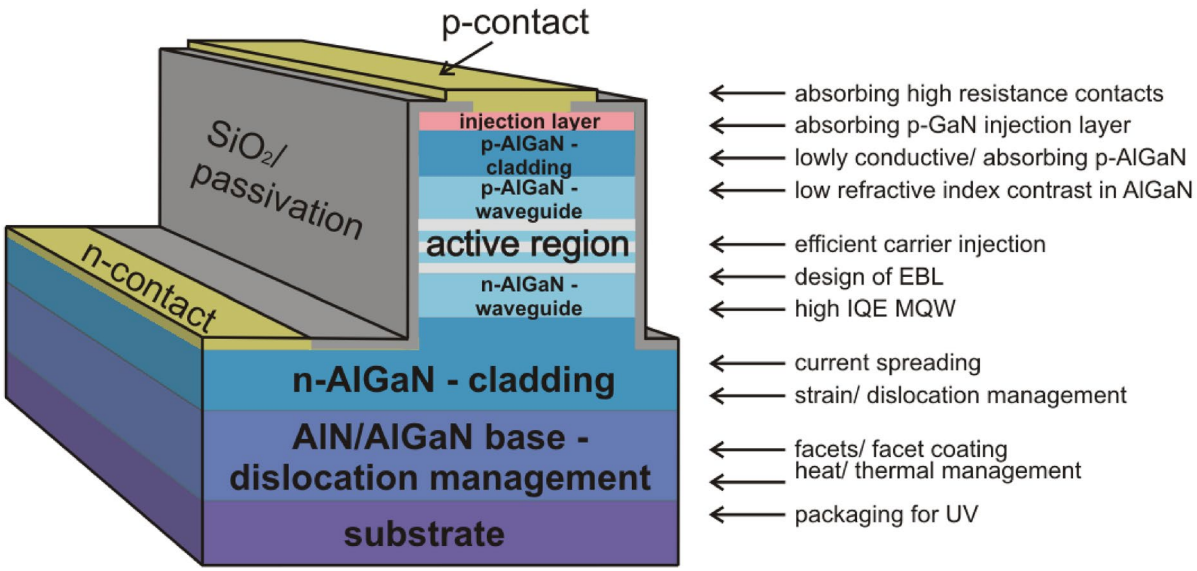

Figure 2: Standard UV laser diode design and main challenges that need to be addressed to achieve electrically injected lasing (adapted from Ref. [51]).

formation, band alignment, and absorption. P-type doping of AlGaN is achieved using Mg, and for GaN and Ga-rich AlGaN, resistivities in the range of 1 Ωcm have been demonstrated [52, 53]. For higher Al content, the activation energy of the Mg-acceptor seems to increase and incorporation of compensating point defects, such as nitrogen vacancies, is promoted [54]. This makes p-type doping of Al-rich AlGaN and achieving relevant p-conductivity even more challenging. Best resistivities are ranging around 50 Ωcm, which is not only a challenge for carrier injection but presents also a significant heating source [54]. A potential solution for this is polarization doping; however, its underlying mechanisms are not fully understood [48, 55].

High Schottky barriers to Al-rich AlGaN normally result in poor ohmic contacts [56]. Hence contacts to the laser diode are typically not made to the p-cladding layer but rather to a GaN:Mg hole injection layer. This thin GaN layer allows for ohmic contacts with low contact resistance and efficient carrier injection [57, 58]. Unfortunately, GaN is absorbing the desired UV laser light, which can increase the laser threshold or even prevent the diode from lasing [59, 60]. This challenge, while unique to the UV diode lasers, can be addressed by either making the p-GaN layer thin, making the p-cladding layer thick, or making contacts to p-AlGaN and thus abandoning the GaN layer [61]. Each solution has its own pros and cons and will be discussed below. In addition to the p-GaN absorption, some absorption from the p-AlGaN layer is expected as well [47, 48]. Finally, the waveguide needs to be designed to have enough Δn (n is the index of refraction) compared to the cladding layer to provide for optical mode confinement and waveguiding [62, 63]. This can be rather challenging for Al-rich AlGaN as Δn is dependent on composition contrast between the cladding and waveguide and increasing the composition of p-AlGaN cladding results in rapidly degrading resistivity and associated losses. Hence, typically, $\Delta n < 0.05$ between the waveguide and cladding layer needs to be considered for wave confinement in realistic laser structures [64–66].

The active region consists of the MQW and an electron blocking layer. For AlGaN UV laser diodes, many of the design rules known from LEDs and visible laser diodes can be applied. Here, the main challenges lie in the actual growth of the quantum wells and barriers, carrier confinement and injection, and to some extend in the design of the electron blocking layer. The importance of the MQW design and growth can be seen in optically pumped laser diodes, where laser thresholds can diverge by orders of magnitude even when grown on templates with comparable dislocation densities [67].

For UV laser diodes emitting at wavelengths < 240 nm, the polarization of the MQW emission needs to be taken into account when laser diodes are designed. Since the valence band ordering in AlGaN switches, a crossover point from the TE (transverse electric) to TM (transverse magnetic) polarized emission is typically found around that wavelength; however, the exact transition wavelength depends on the strain in the layers [68, 69].

The n-side of the laser diode is seemingly the one with the least concerns. n-type doping of AlGaN has been established for Al contents of up to 80% [70–73]. Electron injection is achieved using Ti, Cr, or V-based contacts and ohmic contacts have been established independently by many groups [74, 75]. The main challenge for the n-side is to achieve thick AlGaN layers without relaxation and to provide sufficient conductivity to support high current density in the laser diode.

Lastly, AlGaN-based laser diodes have some challenges related to fabrication. The general fabrication steps needed to transform epitaxial layers into electrically addressable devices have been developed as part of the UV LED research [61, 76–78]. However, some other fabrication steps that need to be improved for the demonstration of cw UV laser diodes are still pending; these include: reliable cleaving, facet coating with highly reflective mirrors, passivation schemes, and UV transparent packaging solutions. Also, heat transport and heat dissipation are rarely investigated for AlGaN-based devices including laser diodes, but it will be important considering the expected current densities to achieve cw UV lasing.

Native substrates for UV laser diodes

It is well recognized that the dislocation density (DD) in the active region has a tremendous impact on the efficiency and performance of the MQWs in any optoelectronic device. This is illustrated by the work of Ban et al., who demonstrated that for all UV wavelengths addressable with AlGaN the internal quantum efficiency (IQE) is a function of dislocation density (Figure 3) [37]. Only when the DD is reduced to $< 10^7$ cm^{-2}, IQEs exceeding 95% can be achieved [46]. In addition, it is found in UV LEDs that dislocations can lead to a degradation of the light output especially at higher output power (driving current density) and that the operation lifetime (measured as output intensity decrease below 70% of the initial output) can be less than 20 h when grown on sapphire or other templates with dislocation density ~ 1×10^9 cm^{-2} [79]. Lastly, as mentioned before, the only electrically injected conventional laser diode and the lowest optically pumped laser thresholds in the UVC region were achieved on AlN substrates [8, 38].

Therefore, it is concluded that high-quality AlGaN active regions and laser diodes can only be achieved by lowering the DD from 10^{10} cm^{-2} on sapphire by at least two to three orders of magnitude. Technologically feasible solutions to reduce dislocations are: (a) high temperature annealing of AlN, (b) superlattices on AlN/sapphire template, (c) use of epitaxial lateral overgrowth (ELO), or (d) the use of native GaN and AlN substrates for low and high Al content AlGaN, respectively, as discussed in

TABLE 2: Lattice parameters and properties for substrates typically used in the growth of AlGaN.

	Sapphire [80]	AlN [81–83]	GaN [84–86]
a-axis [Å]	4.765	3.1129	3.1878
c-axis [Å]	12.982	4.9819	5.185
RT-thermal expansion coefficient [10^{-6} 1/K]	5.0 (a-axis) 9.0 (c-axis)	4.2 (a-axis) 5.3 (c-axis)	5.59 (a-axis) 3.17 (c-axis)
Thermal conductivity [W/cm K]	0.23 (c-axis) 0.25 (a-axis)	3.2	2.1
UV-Transparency	Excellent	Excellent	Poor
Price	Low	High	High
Availability	Excellent	Poor	Good
Mismatch to GaN	16.1%	2.2%	–
Mismatch to AlN	13.3%	–	2.2%

*Mismatch calculations for sapphire account for 30° lattice rotation at the interface.

the following. Table 2 give an overview over the lattice parameters for substrates typically used for the growth of AlGaN.

In 1862 Briegleb and Geuther were the first to synthesize AlN by heating of aluminum fillings under nitrogen gas flow. The observed increase of weight indicated that Al and N had reacted to form AlN [87]. Slack et al. were the first to work on the controlled synthesis of AlN in the 1970s. It was suggested that growth via sublimation in a closed tungsten crucible or in an open tube with a gas flow would lead to single crystal AlN [88]. Initial experiments produced millimeter-sized AlN crystals. Subsequently, these experiments were extended to grow AlN crystals by the Al pellet drop method in a tungsten crucible in an rf-heated tungsten furnace under nitrogen atmosphere and crystals of up to 1 cm in length and 0.3 cm in diameter were achieved [89]. Very few new efforts in AlN crystal growth were undertaken in the 1980s and beginning of 1990s. However, shortly after the successful p-doping of GaN and the first available GaN-based LEDs, an increased interest was given to AlN.

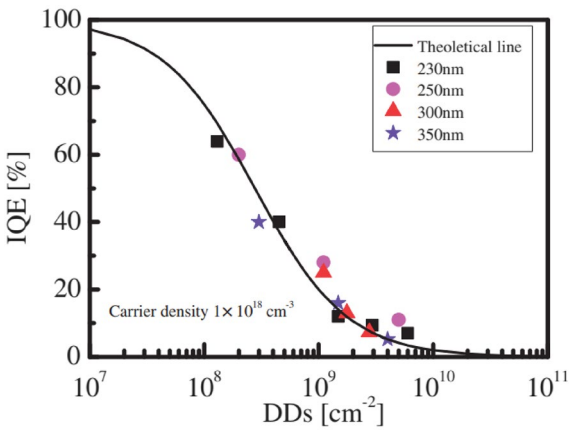

Figure 3: IQE as a function of DD in an underlying layer for MQWs with different emission wavelength. The IQE starts increasing significantly only for dislocation densities < 10^8 cm^{-2} [37].

This led to a renaissance of layer and later bulk growth of AlN at the end of the 1990s [90].

While other methods such as hydride vapor phase epitaxy (HVPE) growth and solution growth of AlN were explored, over the years physical vapor transport (PVT) has been established as the most promising technique for high-quality AlN substrates. For PVT or sublimation growth, AlN powder is contained in a crucible (source) which is inductively heated. Due to the high applied temperature (> 2000 °C), the AlN is non-congruently sublimed:

$$AlN^{solid} \leftrightarrow Al^{gas} + \frac{1}{2}N_2^{gas}$$

Opposing to the crucible a seed is positioned which is heated to temperatures slightly lower than the source. The thermal gradient between seed and source results in diffusion of the sublimed gas molecules leads to the growth of AlN via a reverse reaction. Despite the fact that bulk AlN crystals theoretically can be grown at temperatures as low as 1800 °C and as high as 2500 °C, temperatures around 2200 °C are more favorable in order to achieve high growth rates and good crystal quality [88, 91–93]. In addition to source and seed temperatures, the temperature gradient between these two is an important parameter for the control of transport and growth rate. Typical values for the temperature gradient are around 50 °C/cm. With these reactor parameters, growth rates in the c-direction between 50 µm/h (1800 °C), and 1 mm/h (2300 °C) can be achieved [92, 94]. However, high growth rates may lead to a reduced crystal quality so that growth rates are usually maintained at several hundred µm/hour.

The structural quality of the grown AlN crystals obtained by PVT depends directly on the type and quality of seed crystals. Seed crystals are needed to provide structural information for the condensing Al and N atoms, including polarity and orientation. The first results for SiC seeded growth were presented in 1996 by Balkas et al. [90]. The crystals grown during these first

attempts showed cracks and incorporation of Si and C. As an alternative and because native seeds were initially not available, self-seeding was proposed [89]. For self-seeding, a small growth target was used, typically a conical tube, to limit the number of stable nuclei [95]. However, due to the randomness of the grain selection process, and constrained growth environment, the resulting crystals were small, randomly oriented, and had relatively high dislocation density [96]. The best and nowadays most widely spread solution to overcome seeding related concerns is the use of native seeds. These seeds are typically obtained by spontaneous nucleation and growth of Lely-like, c-oriented platelets close to equilibrium conditions. First attempts using native seeds resulted in transparent crystals with XRD rocking curve FWHMs as low as 25 arcsec [92]. By establishing a procedure which includes the growth of an AlN boule, cutting and polishing a wafer from that boule, and subsequent re-growth on that wafer, Noveski et al. established a procedure which led to increased native seed size over time [97]. Using this procedure, wafers with diameters exceeding 56 mm are available nowadays.

For Ga-rich AlGaN layers low dislocation GaN substrates are used. The dominating techniques to achieve low dislocation density substrates are HVPE growth and growth via the ammonothermal technique. An excellent review over GaN HVPE and ammonothermal growth can be found elsewhere [98].

AlN and GaN single crystal substrates with dislocation densities in the 10^6 to 10^7 cm^{-2} range are possible by exploiting hydride vapor phase epitaxy in combination with sapphire substrates [99–101]. Even the growth of AlGaN substrates is possible using this technique [102]. Lower dislocation density native substrates are only available from ammonothermally grown GaN, HVPE, and physical vapor transport grown AlN in combination with native seeds. These techniques can achieve dislocation densities < 10^3 cm^{-2} range [91, 103–105].

Growth of AlGaN epitaxial layers and UV laser structures

Growth of AlGaN layers on sapphire using MOCVD or MBE has been pursued since the mid-80 s. The first breakthroughs were made when low temperature AlN or GaN buffer layers were used. Ponce et al. demonstrated growth of $Al_{0.5}Ga_{0.5}$ N with dislocation densities in the 10^{10} cm^{-2} range [106]. In general, for the direct growth on sapphire, improvements in the dislocation density and relaxation are possible by adjusting the buffer layer growth and annealing conditions, inclusion of a high temperature AlN template, or thicker growth, but the lowest dislocation densities achieved are still in the low to mid-10^9 cm^{-2} range [107, 108]. This dislocation density is way too high to achieve electrically injected lasing or even high power UVC LEDs, which resulted in several approaches to reduce dislocation densities using either ELO or AlN/AlGaN superlattices to relax the GaN/AlN/sapphire layers [109–111]. Wang et al. reported that a reduction of the dislocation density in AlGaN films down to the mid-10^8 cm^{-2} is possible by using AlN/AlGaN superlattices, which subsequently allowed for the fabrication of UV LEDs [109, 112]. The effect of using superlattices is explained by their coherent growth, which exerts compressive strain for the thick upper AlGaN films and eliminates cracking [113]. Similar results were recently demonstrated by Fukuyama et al. using high temperature annealing of AlN templates grown on sapphire [114]. Annealing of AlN templates in N_2 and/or N_2–CO gas atmosphere at 1700–1750 °C for 0.5–4 h resulted in dislocation densities in the low 10^8 cm^{-2} range and crack free films with thicknesses exceeding 3 µm. Deposition of AlGaN films on annealed AlN seems possible; however, the formation of Al–O–N needs to be controlled [115, 116]. The underlying mechanism for the reduction in the dislocation density has been explained only recently. Vacancy core diffusion-controlled dislocation climb was identified as a dominant recovery mechanism in high temperature annealing of AlN heteroepitaxial films while dislocation annihilation mechanisms via dislocation glide and vacancy bulk diffusion were found to be less significant [117]. Despite the great reduction in dislocation density, high temperature annealing of AlN has not been established as a mainstream approach to grow high efficiency LEDs or even laser. This could be related to yield issues and challenges related to the growth of AlGaN on top of these templates [118].

As an alternative to relax AlGaN and to reduce dislocation density, growth on pretreated templates was tried by several groups. This includes the growth on epitaxial lateral overgrowth (ELO) templates, nano-patterned sapphire templates, and growth on templates using plastic relaxation through buried cracks [110, 119, 120]. Interestingly, the achieved dislocation density for all these techniques is around mid-10^8 cm^{-2} at best. While these dislocation densities are low enough to achieve optically pumped UV lasing and electrically pumped lasing in the visible and more recently in the UVA [121] wavelength range, electrically injected lasing in the UVB and UVC range on these templates has not been demonstrated.

AlGaN films grown on GaN substrates will be under tension and crack easily for any appreciable Al content. Therefore, very few efforts have been made to grow thick, Ga-rich AlGaN layers or even UV optoelectronic devices on GaN substrates [122, 123]. If thicker AlGaN layers are desired, a relaxation mechanism needs to be invoked to prevent cracking. One possible pathway is facet controlled epitaxial lateral overgrowth (FACELO) which leads to the generation of misfit dislocations at the GaN/AlGaN {11-22} interface and relaxation [124]. It is yet to be demonstrated that such a process can lead to better devices than growth on AlN/sapphire templates.

Since AlGaN growth on AlN substrates is under compression, cracking is not expected from these layers despite the lack

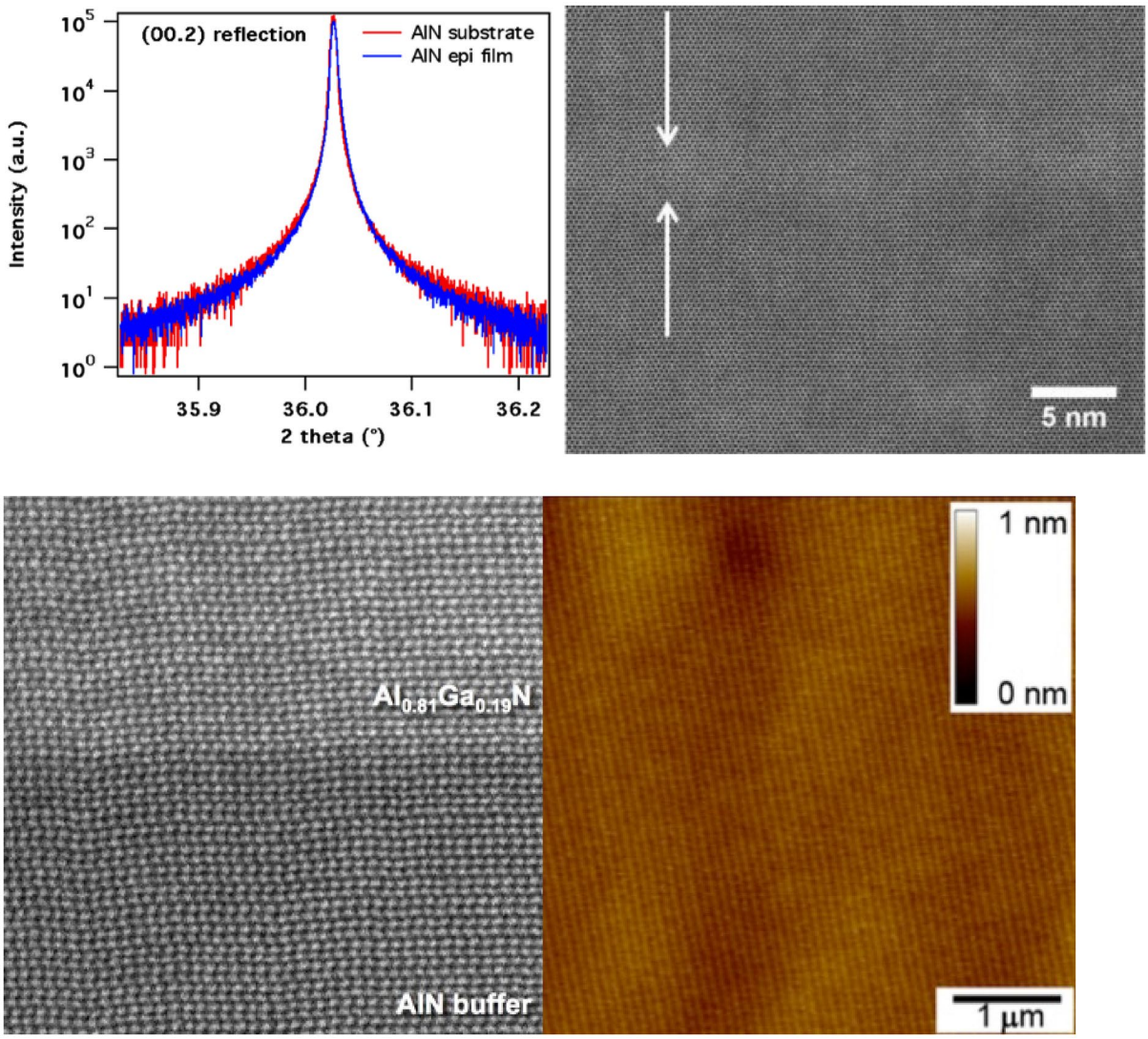

Figure 4: 2θ-ω X-ray diffraction scan of an AlN homoepitaxial layer in comparison with the substrate (top left) and HRTEM of an homoepitaxial AlN film showing perfect lattice continuation across the interface (marked with arrows) (top right). HRTEM micrograph for AlGaN on AlN for a nominal 80% Al content; no dislocations were observed at the heteroepitaxial interface or in the AlGaN (bottom left). 5 × 5 µm^2 AFM image of $Al_{0.7}Ga_{0.3}N$ grown on vicinal (0001)-oriented AlN. The surface consists of the desired bilayer steps with an RMS roughness of less than 50 pm (bottom right).

of relaxation. Therefore, Al-rich (Al > 70%) AlGaN layers grown on either HVPE or PVT substrates grow pseudomorphically with dislocation densities in these layers being the same as in the substrates. This is indicated by the images in Fig. 4. For a homoepitaxially grown AlN film, triple-axis, high-resolution x-ray diffraction measurements of the (0002) Bragg peaks of the thin films indicate that it is epitaxial and strain-free, as evidenced by a perfect alignment and equal width of 15 arcsec of the substrate and film rocking curves (Fig. 4—top left) [125]. Atomic force microscopy characterization for such AlN films shows step-flow growth along the terraces for AlN films deposited at 1250 °C [126]. No pitting or V-defect formation was observed in these films [127]. High-quality homoepitaxy is further evidenced by transmission electron microscopy (TEM) and high-resolution TEM (HRTEM) studies, which both confirmed perfect epitaxy (Fig. 4—top right).

Similar observations are made for AlGaN layers grown on AlN substrates [126, 128]. An HRTEM micrograph of AlGaN on AlN, imaged along the [11–20] zone axis, is shown in Fig. 4 (bottom left) for a nominal 80% Al content. No dislocations are observed along the heteroepitaxial interface between the AlGaN and the AlN homoepitaxial layers in the viewable area. In addition, an AFM image of AlGaN grown on vicinal (0001)-oriented AlN is shown in Fig. 4 (bottom right). The surface consists of bilayer steps with an RMS roughness of less than 50 pm. Both results confirm that high aluminum content AlGaN films grow pseudomorphically on AlN without introduction of new, strain-relieving dislocations [128, 129].

By establishing the growth of pseudomorphic AlGaN layers in the range of 50–100% Al content on single crystal AlN substrates, the growth of high-quality AlGaN/AlGaN multi quantum wells becomes possible. STEM imaging of an MQW structure with 55% Al content in the wells and 65% Al content in the barriers reveals that the interfaces between the waveguide, wells, and barriers are atomically smooth and no inhomogeneity in the AlGaN layers is observed [38].

Doping of AlGaN

A high free carrier concentration is desired in both n-type and p-type regions to support charge carrier transport and contact formation. Both these factors are critical for lowering ohmic conduction losses and improving wall-plug efficiency by achieving electrical-injected lasing at lower input power. Thus, understanding the doping of III-nitride materials to achieve a high free carrier concentration in the epitaxial films is a crucial aspect for success of UV lasers. The following subsections describe the current status of doping in AlGaN for UV lasers.

n-Doping

Si is typically used as donor in all III-nitride materials. It exhibits a very low donor activation energy (≈ 15 meV) in GaN and AlGaN for Al compositions < 80% [9]. Accordingly, free electron concentrations of the order of 10^{19} cm^{-3} can be routinely achieved using Si-doping [70, 130, 131]. For GaN on sapphire, beyond a free carrier concentration of 4×10^{19} cm^{-3}, Si-doping introduces a strong tensile strain in the GaN layer due to dislocation climb related to Ga-vacancies. This leads to formation of cracks and rendering epitaxial layers useless for device growth [132]. For native GaN substrates, due to the low dislocation density, this tensile strain related to Si-doping is not of concern. However, for both substrates compensation at high doping levels needs to be considered when limitations are assessed. Alternatively, Ge doping of GaN/sapphire has been shown to result in a free carrier concentration exceeding 1×10^{20} cm^{-3} [130, 133]. The positive impact of Ge doping on optoelectronic device has yet to be explored. Anyways, achieving a high free carrier concentration in n-GaN and Ga-rich AlGaN can be considered a matured technology.

N-type doping of Al-rich AlGaN is still a major challenge. There are two primary factors limiting doping in Al-rich AlGaN: (a) seemingly increased activation energy and (b) compensation. A sudden increase of Si donor activation energy in n-$Al_xGa_{1-x}N$ as x increases beyond 0.8 has been observed, as shown in Fig. 5a [134]. Si in Al-rich n-AlGaN does not behave as a shallow donor; it presumably undergoes a deep-acceptor (DX) transition with increasing Al composition in the AlGaN film [135]. Recent results indicate shallow donors in Ga-rich AlGaN actually undergo a deep donor transition instead of a deep-acceptor DX [71]. Anyways, this transition is seen as a high carrier activation energy. In principle, higher activation energy may be overcome by increased doping levels by mini-band formation or screening effects assuming a deep donor transition. However, with an increase in Si-doping beyond a critical concentration, the free electron concentration reduces in the Al-rich AlGaN as a consequence of the second major challenge, i.e., increased compensation [136]. Harris et al. have reported on the formation of $V_{Al} + nSi_{Al}$ complexes acting as compensators in highly-doped Al-rich n-AlGaN films as the source of the observed self-compensation [137]. Thus, Si-doping results in a

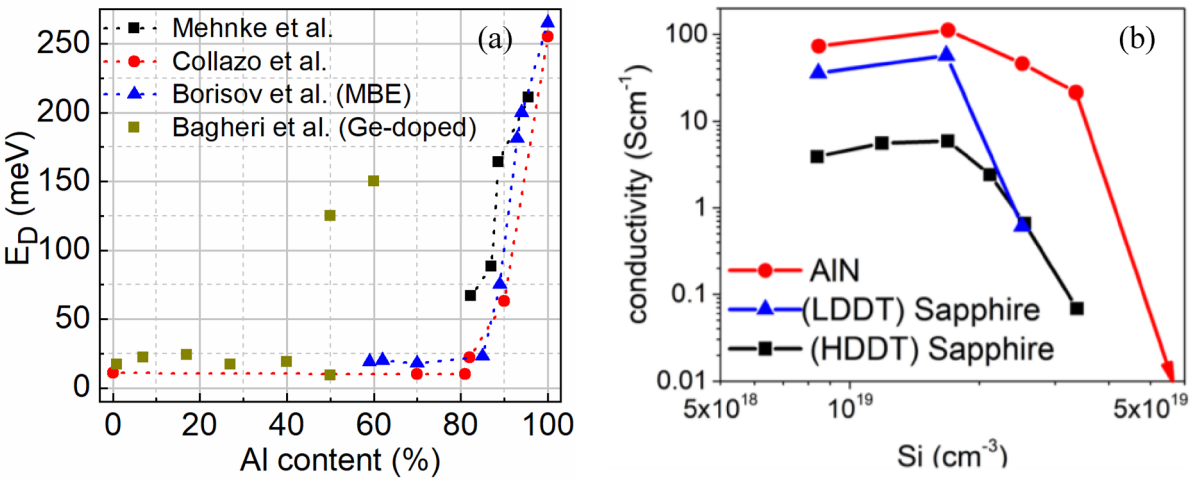

Figure 5: (left) Comparison of activation energy in AlxGa1-xN obtained from different literature [9, 71, 139, 140], and (right) conductivity of Si-doped $Al_{0.7}Ga_{0.3}$ N showing the "knee behavior" with Si-doping concentration [134]. A positive impact of a native AlN substrate (red) and low dislocation density template (LDDT—blue—10^8 cm^{-2}) was found compared to a standard, high dislocation density template (HDDT—black—10^{10} cm^{-2}) was found.

"knee behavior" in the resistivity of the Al-rich n-AlGaN films, as shown in Fig. 5b [138]. Further, even at low doping, carbon and vacancy-oxygen complexes act as acceptor-type compensating point defects at densities higher than those observed in GaN [70]. Hence, control of compensating point defects is necessary to achieve a high free carrier concentrations in the Al-rich n-AlGaN films. This is typically achieved by controlling the chemical potential of the growth and impurity species via reactor pressure, V/III ratio, temperature, carrier gas, etc., or by controlling the electrochemical potential via minority carrier generation during growth [45, 73, 131, 138].

Traditionally, AlGaN films grown on sapphire substrates suffer from high DD due to the lattice mismatch. In addition, Bryan et al. have shown that the compensating point defect incorporation is a strong function of the threading dislocation density (TDD) [134]. Hence lowering TDD, by growing on native substrates is expected to increase doping efficiency. Accordingly, it was reported that the lowest DD ($< 10^3$ cm^2) achieved by growing Al-rich n-AlGaN on single crystal AlN substrate resulted in orders of magnitude higher free carrier concentration as compared to films grown on sapphire under similar conditions, Fig. 5b. A similar, albeit smaller, effect was observed on low DD AlN templates [134].

As an alternative to conventional n-type doping, either the use of superlattices or polarization doping has been proposed [141–144]. The first approach exploits that the composition modulation of a uniformly doped ternary semiconductor can enhance the donor/acceptor activation and is primarily used in low Al content devices. It often also serves as a relaxation scheme a described before [112]. For superlattices, n-type conductivities with free carrier concentrations in the 10^{19} cm^{-3} range have been demonstrated. Similar results were achieved for polarization doping using graded layers. Here, grading AlGaN exploits that the polarization of the layer can field-ionize the acceptor/donor dopants efficiently at room temperature. However, at least on the n-side, superlattices and polarization doping are rather uncommon approached due to the success of conventional n-type doping in AlGaN:Si and challenges in achieving n-type contacts to these layers.

Nevertheless, all these results point toward the importance of and research required to understand the point defect control and growth of high-quality epitaxial films with low TDD for improved free carrier concentrations and better contact formation in Al-rich n-AlGaN films for future UV laser diodes.

p-Doping

Mg is the only known acceptor impurity that can be easily incorporated into GaN and AlGaN during the growth and allows for reasonably high hole concentrations [52, 145, 146]. While passivation of Mg by hydrogen has been solved through the seminal works by Amano et al. and Nakamura et al. [52, 147], self-compensation is still a major challenge at high Mg concentrations when grown on foreign substrates, primarily due to the formation of nitrogen vacancies, thereby limiting the maximum hole concentration in the p-GaN film. Consequently, the relatively high acceptor activation energy of Mg lying in the range of 120–200 meV results in typical peak hole concentration in p-GaN films grown on foreign substrates using MOCVD in the range of 10^{17}–10^{18} cm^{-3} [148]. The difference in carrier concentrations between the n-type and p-type GaN along with a significantly lower hole mobility compared to the electron mobility results in a greatly lowered charge balance efficiency in laser diodes resulting in increased threshold currents and low injection and wall-plug efficiencies [53].

One way to enhance free hole concentration in p-GaN is low temperature growth. Typically, NH_3 is used as a precursor gas for the growth of GaN, and is a source of H, which forms a neutral complex with Mg during the high temperature MOCVD growth [149]. Hence, thermal activation is usually performed to reduce the hydrogen concentration and increase the free hole concentration in p-GaN. On the other hand, low temperature growth techniques such as molecular beam epitaxy (MBE) or pulsed sputter deposition (PSD) has been demonstrated to show significantly lower hydrogen content in the p-GaN films [149, 150]. Accordingly, free hole concentration exceeding 10^{18} cm^{-3} can be achieved (even without any post growth treatment) in low temperature MBE-grown p-GaN films [151]. Other ways to achieve a higher free hole concentration is to reduce compensating point defects like nitrogen vacancies in p-GaN [53]. This can include control of the growth condition (supersaturation) or other approaches including defect quasi Fermi level control [152]. Finally, growth of p-GaN on single crystalline AlN substrates has been shown to mitigate the typically observed nitrogen vacancy-related blue luminescence in PL spectra [145, 153]. As a result, p-GaN films grown on AlN substrates using MOCVD showed nearly an order of magnitude high free hole concentration (~ mid-10^{18} cm^{-3}) [53]. The relation between compensating defects and dislocations in p-GaN (and p-AlGaN) has yet to be clarified.

Mg doping in AlGaN is still not well understood with no clear consensus on fundamental properties, including the activation energy or type of conduction. Initial reports by Suzuki et al. and Li et al. indicated increasing activation energy with increasing Al composition, resulting in higher resistivities in p-AlGaN in comparison to p-GaN [154, 155]. However, the studies were limited to Ga-rich compositions. A similar conclusion was made for Al-rich $Al_{0.75}Ga_{0.25}N$ grown on AlN with a large activation energy of ~ 400 meV and resistivity > 1 kΩcm even at elevated temperatures (100 °C). Recently, Kinoshita et al. reported on a low activation energy (< 50 meV), albeit with hopping conduction, in Mg-doped Al-rich AlGaN, resulting in a

resistivity of ~ 50 Ωcm; however, this is significantly larger than that of p-GaN at ~ 1 Ωcm [54]. Aoyagi et al. have also reported on a low activation energy (75 meV) in p-$Al_{0.4}Ga_{0.6}$ N using pulsed supply of source gases during the MOCVD growth [156]. Similarly, the activation energy of Mg-doped p-AlN nanowires was reported to be ~ 23 meV [157]. It is interesting to note that recent reports on the activation energy in p-AlGaN are lower than p-GaN. Although low activation energies were reported, the resistivity is consistently orders of magnitude higher than that of p-GaN due to a significantly reduced hole mobility. The high resistivity is a major challenge and a source of large ohmic losses and associated heating at high current densities needed for lasing. Further, the variations in the reported values indicate the uncertainty in p-AlGaN properties. Hence, p-type doping of Al-rich AlGaN should be an important focus of research, essential for the implementation of AlGaN-based laser diodes.

A major challenge that arises in conventional Mg-based p-doping in addition to high resistivities discussed in the previous section is the Mg or impurity-based absorption losses [47]. Consequently, alternatives to regular doping have also been studied. For example, growth of superlattice structures are a popular technique to achieve a high free hole concentration in p-AlGaN [158]. A short period superlattice (SPSL) consists of several thin Mg-doped AlGaN films with alternating Aluminum content instead of a bulk p-AlGaN film [159]. The periodic oscillations of the valence band due to short periods of p-AlGaN layers may lead to tunneling of holes from the acceptor level in the higher bandgap layer into the valence band of the lower bandgap layer. Consequently, the effective activation energy is reduced, and the SPSL p-AlGaN films show a significantly improved conductivity [160]. Another promising technique is the polarization-induced doping and is discussed in the following section.

Polarization-induced p-doping

So far, the only working electrically injected UVC laser diode with edge emission is based on polarization doped AlGaN layers on the p-side of the device [8, 59]. Therefore, this technique demands an in-depths discussion. The basic idea of polarization doping and graded AlGaN is that by creating a compositionally graded layer in AlGaN, a gradient in the dipole moment and associated polarization charge are generated. The gradient results in a net uncompensated charge given by:

$$\rho_\pi = \nabla\left(\vec{P}_S + \vec{P}_P\right)$$

where P_S is the spontaneous polarization and P_P is the piezoelectric polarization. For wurtzite AlGaN, spontaneous polarization is directed along the -c-axis, i.e., toward the N-polar face. Calculation or measurement of the polarization coefficient is challenging and exact values are still under discussion. A good discussion about this topic can be found elsewhere [161]. Nonetheless growth along c-axis, with Ga molar fraction increasing along the growth direction, the divergence of the spontaneous polarization vector in equation is negative. The requirement of a charge neutrality requires a similar density of positive charge carriers, which may be mobile holes or immobile ionized point defects (intrinsic or extrinsic). Interestingly, for the n-type polarization-induced doping, as seen in the 2D electron gas (2DEG)-based HEMTs, the charge neutrality is achieved via free electrons and a separate dopant source is unnecessary, with the source of the 2DEG hypothesized to be the surface. 2D hole gases in III-nitrides were only recently observed by Chaudhuri et al. and the authors stressed the importance to control the compensation level and sharpness of the interfaces [162]. However, doping was also not necessary to achieve 2D hole gases. In contrast, for graded layers, acceptor (Mg) doping seems necessary to provide the mobile charge carriers, i.e., holes to account for charge neutrality. The graded layer may be partly Mg doped as was the case with first demonstrated UVC laser or the adjacent layer may be Mg doped [59]. Accordingly, assuming a polarization charge density of ρ_π/q, the sheet hole concentration is then given by

$$n_s \approx \frac{1}{q}(t - w)\rho_\pi$$

where t is the thickness of the graded region, and w is the thickness of the depletion region. Hence for a known composition grading and thickness, the polarization charge density and sheet hole concentration may be estimated.

Polarization-induced doping in conjunction with Mg doping offers two primary advantages over conventional Mg doping: (a) zero activation energy for the hole concentrations required to compensate the polarization charge, i.e., a temperature-independent high hole concentration ensuring low resistivities [55], and (b) the Mg-doped region (source of holes as countercharge for the polarization charge) can be separated from the graded region with polarization charge, which can then be employed as undoped cladding, thereby reducing modal losses [48, 59].

Most visible, UVA, and UVB lasers demonstrated in the literature so far do not need polarization doping to operate; they typically simply reduce p-doping to avoid absorption-related losses in the waveguide and cladding. On the other hand, so far, the only electrically injected UVC laser is heavily dependent on polarization doping [8], which may point to the importance of that technology for the UVC range.

Carrier injection layers and contacts

Robust contacts with low specific contact resistance are necessary for laser diodes due to the requirement of very high current densities that enable overcoming the electrical lasing

threshold. While this may not be of concern for laser diodes based on GaAs/AlGaAs and GaN/InGaN systems, it is of prime importance, especially when transitioning from UVA to UVC regimes, where in Al-rich AlGaN, high electron and hole barriers at the charge neutrality levels (Fermi level pinning) at the surface of AlGaN present a substantial challenge to an efficient carrier injection [56]. As a consequence, many approaches have been employed or proposed that may be broadly grouped into two categories: (a) contacts to n-AlGaN on one terminal and (b) hole injection layers, tunnel junctions and contacts to p-AlGaN on the other terminal.

n-Contacts

The contacts to n-GaN or Ga-rich AlGaN films are a mature technology and are implemented in visible and UVA emitters [163, 164]. A Ti/Al-based contact metallization scheme with rapid thermal annealing is the most commonly used to form the ohmic contact to n-GaN or Ga-rich n-AlGaN. While Fermi level pinning due to surface states results in a Schottky barrier at the Ti/n-GaN interface, it is believed that a high temperature anneal enables Ti to extract N from the GaN via the formation of TiN at the Ti/n-GaN interface [164]. The resulting donor type nitrogen vacancies generated in the underlying GaN film result in large electric fields at the interface, narrowing the depletion region and allowing electrons to tunnel from the metal to GaN, and vice-versa [165]. This mechanism allows achieving an ohmic contact to n-GaN or Ga-rich AlGaN with very low contact resistances. A specific contact resistance of the order of 10^{-6} Ωcm^2 has been reported for GaN and Ga-rich $Al_xGa_{1-x}N$ ($0 \le x \le 0.35$) [164]. Further reduction in contact resistance is possible by using surface treatments. Reactive ion etching (RIE) of n-type GaN before contact deposition has been shown to introduce additional nitrogen vacancies at the GaN surface. The surface thus becomes highly n-type, and further lowers the contact resistance [166].

However, the formation of ohmic contact to Al-rich n-AlGaN is a major challenge due to the increasing Schottky barrier height and the Fermi level pinning (charge neutrality level) with increasing Al composition [56]. The typically used Ti/Al-based metallization scheme shows the presence of a Schottky barrier at the metal/n-AlGaN interface [167]. Accordingly, the contact formed on Al-rich n-AlGaN shows a very high contact resistance. As a possible solution, Pt/Au, V/Al, Zr/Al, Nb, etc.,-based contact schemes have been shown to offer a significantly lower contact resistance as compared to the Ti/Al-based metallization [168–170].

Another major approach to lower the contact resistance is to achieve a high doping and free carrier concentration in the Al-rich n-AlGaN films which may enable low contact resistances [167, 171]. For example, the growth of Al-rich n-AlGaN films on single crystalline AlN substrates (DD < 10^3 cm^{-2}) has been shown to offer orders of magnitude higher free electron concentration due to a reduction of dislocation related compensators [171]. Consequently, the V/Al-based contacts to Al-rich n-AlGaN grown on AlN substrates show orders of magnitude higher current than similar composition n-AlGaN films grown on foreign substrates.

However, these higher currents through AlGaN films grown on AlN substrates are observed only at higher voltages (≈ 5 V) where field emission is the dominant current conduction mechanism. At low voltages (< 5 V), it was observed that the Al-rich n-AlGaN films grown on AlN substrate show orders of magnitude lower current conduction than the films grown on foreign substrates, as shown in Fig. 6 [167]. Primary reason for this lower current is attributed to the lower defect density in AlGaN films grown on native AlN substrate resulting in a low trap-dominated conduction mechanisms. However, surface treatments such RIE is believed to introduce a higher trap density underneath the contact interface thereby improving the currents through the contacts at lower voltages, as observed for current through etched surface in Fig. 9. Therefore, apart from adopting native AlN substrates that can offer a significant improvement in the free carrier concentration in the epitaxial film, understanding the surface treatments and their effects in minimizing the contact resistance is necessary to obtain a low contact resistance in Al-rich AlGaN films. It is clear that work on ohmic contacts to Al-rich n-type AlGaN is ongoing with many possible pathways being explored.

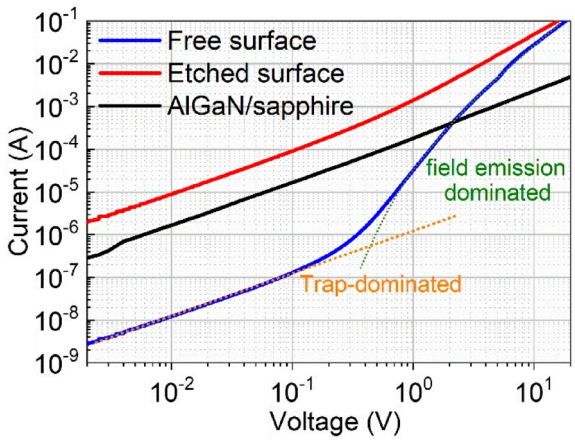

Figure 6: Current through V/Al-based contacts to n-$Al_{0.7}Ga_{0.3}$ N on sapphire substrate (AlGaN/sapphire), AlN free surface and RIE treated AlN etched surface [167]. Contacts in this study had transfer length measurement (TLM) geometry, whereas AlGaN films corresponding to free surface and etched surface were grown on native AlN substrate.

p-Contacts

Direct contacts to p-AlGaN, especially on the Al-rich side, are an enormous challenge due to an extremely large hole barrier at the charge neutrality level and challenges in effective p-doping, as discussed earlier [56]. Consequently, most of the III-nitride emitters rely on p-GaN as a contact and hole injection layer into p-AlGaN irrespective of the emission wavelength [172]. However, strictly speaking, low resistance ohmic contacts to p-GaN are still elusive [172, 173]. The Fermi level pinning at about 1.4 eV above the valence band, compared to 0.6 eV below the conduction band on n-GaN, and the resulting higher Schottky barrier greatly impacts the contact resistance [174, 175]. A Ni/Au contact metallization scheme is typically used to form ohmic contacts to p-GaN [173]. Although a few authors reported on the p-GaN contact resistance of the order of 10^{-5}–10^{-6} Ωcm^2 [176], most reports quote it in the range of 10^{-1}–10^{-3} Ωcm^2 (Fig. 7) [177]. Many models have been discussed to explain the current conduction mechanisms for the Ni/Au contacts to p-GaN. Initially, the contact anneal, either in air or oxygen ambient, was presumed to result in better p-contacts due to formation of semiconducting NiO at the p-GaN surface with aligned valence bands [178–180]. On the other hand, other reports attributed the current conduction to the formation of Ga-vacancies at the metal/p-GaN interface, similar to contacts on n-GaN, where N-vacancies are expected to form [181]. Finally, the observation of post-anneal reversal of Ni and Au in the Ni/Au metallization stack and the concurrent formation of the Au–Ga alloyed clusters [179, 182] indicated that the conduction occurred at isolated clusters due to geometrical field enhancement [179, 183]. In recent work, Sarkar et al. framed a model to address most of the commonly observed mechanisms in Ni/Au contacts to p-GaN [177]. It was proposed that the Ni/Au forms an alloyed contact (or clustered contact) to p-GaN, similar to the contact model originally developed by Braslau et al. for GaAs [184]. Accordingly, the Ni/Au contact anneal in air or oxygen ambient results in the formation of NiO, which allows Au to diffuse through it and reach the GaN surface in isolated clusters. The formation of Au–Ga clusters results in the formation of Ga-vacancies, which offer a lower barrier height compared to the other areas under the contact. Since the conduction occurs at these cluster sites, the contact resistance thus comprises of two contributions: (i) a series resistance in the semiconductor generated by the current crowding around the cluster, and (ii) a metal–semiconductor interface resistance being lower by field enhancement at the clusters. Typically, the field enhancement factor is assumed to be large enough that the contact resistance is limited by the series resistance of the semiconductor and hence the hole concentration.

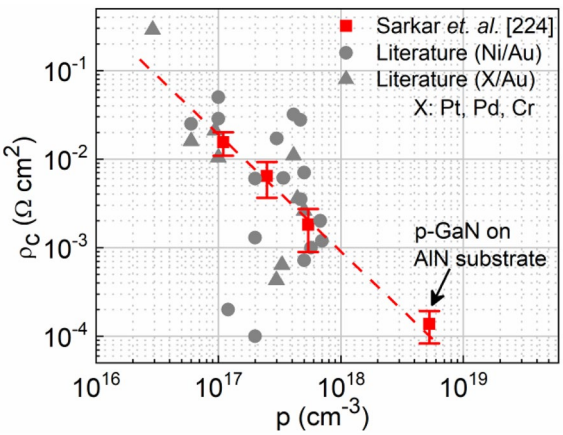

Figure 7: Reported relationship between the contact resistance (ρ_C) and the free hole concentration (p) in p-GaN films [177].

Figure 7 shows the dependence of contact resistance as a function of hole concentration in the p-GaN films. MOCVD-grown p-GaN films (on foreign substrates) mostly show a free hole concentration in the mid-10^{17} cm^{-3} [148], and the corresponding contact resistance lies in the 10^{-2}–10^{-3} Ωcm^2 range. Nonetheless, similar as discussed for n-contact to Al-rich n-AlGaN, it is clearly evidenced that contact resistance to p-GaN is a function of the free hole concentration, which might explain the use of p^{++} contact layer discussed in literature as well [185, 186].

As alternatives to Ni/Au contacts on p-GaN, significant efforts were made to study the feasibility of tunnel junctions and direct contacts to p-AlGaN. The use of highly-doped n-GaN/p-GaN tunnel junctions (TJ) has been demonstrated by several authors [187–189]. During operation, the TJ structure allows for inter-band tunneling between the conduction band of n-GaN and valence band of p-GaN [189]. Note that this requires additional voltage across the reverse biased tunnel junction to allow holes to be injected into the active region [188]. Complications in fabricating such tunnel junctions arise in MOCVD where growth of subsequent GaN films on p-GaN at high growth temperatures suffers from a commonly observed mechanism known as the "Memory effect" [190, 191]. It is believed that the Mg source molecules adsorb on the MOCVD reactor walls during the p-GaN growth. Once the Mg gas source is turned off, the adsorbed Mg from the reactor walls incorporates into the subsequent epitaxial films grown on the p-GaN. Removal of Mg-rich p-GaN surface followed by a low temperature n-GaN re-growth has been shown to strongly reduce the Mg incorporation in the subsequent n-GaN films [191]. In a recent work, Agarwal et al. demonstrated the possibility of suppressing the memory effect using low temperature flow modulated epitaxy (FME) or pulsed MOCVD growth [192]. Prior to the re-growth, the p-GaN surface was exposed to a UV-ozone treatment and an HF etch. The re-grown n-GaN film (on p-GaN) showed a strong reduction of Mg incorporation and a better-quality. Extending the TJs to AlGaN with bandgaps larger than the emission energy, Zhang

et al. demonstrated 292 nm emission using p-AlGaN/InGaN//n-AlGaN TJ [193].

As another alternative, establishing contacts directly to p-AlGaN has also been proposed and studied. Note that the free hole concentration and resistivity are expected to be several orders of magnitude lower and higher, respectively, in comparison to p-GaN, resulting in significant electrical loss in the p-AlGaN layer and contact. In addition, since Ni and Au are both absorbing UV light, the advantages of such contacts are negligible compared to the contact applied straight to a thin GaN film. Using reflective, e.g., Al- or Mo-based contacts, similar to those established in UV LEDs, may increase the barrier too much and make lasing impossible [79]. Despite all these efforts, all lasers demonstrated in the UV range employed p-GaN/Ni/Au-based contacts. Yoshide et al. have successfully demonstrated a 342 nm AlGaN multiquantum well based laser using contacts to thin p-GaN on a relatively thick p-AlGaN [194]. In addition, the recently demonstrated UVC laser diodes also utilized thin p-GaN and a contact to that layer to achieve electrically injected lasing. It is therefore concluded, that for the time being, Ni/Au-based contacts to thin p-GaN layers may still be the most efficient contacts for laser diodes.

Design and technology solutions toward deep-UV lasers

The design of UV laser diodes is challenging due to the inherent materials properties of AlGaN. The challenges that make UV lasers special are diverse since they involve control of optical properties such as waveguiding and control of electrical properties such as low conductivity p-type AlGaN. While the general design of UV laser diodes follows that of visible InGaN laser diodes few attempts have been made to simulate UV laser diodes [59, 60, 195–198]. This is partially because of the missing possibility to confirm theoretical data with experimental data and partially because some fundamental fitting parameters are still unknown or uncertain. The main challenges in the design of UV laser diodes that need to be addressed are: (a) waveguiding and p-GaN absorption, (b) MQW and electron blocking layer design for efficient carrier injection and confinement, and (c) impact of additional optical losses such as impurity related losses and facet related losses on the laser threshold. The following sections will discuss published data regarding these challenges and provide suggestions on how they can be overcome.

Waveguides, p-GaN losses, and optical modes

An essential part for laser diodes is to understand how well the laser mode is traveling in the waveguide and how much light is leaking into the p- and n-side. For UV lasers leakage on the p-side is detrimental since the p-GaN contact layer, if not designed correctly, will absorb the laser light and may prevent lasing at all. Leakage on the n-side is normally only a concern if the n-AlGaN cladding has a large impurity density (leading to absorption losses) or if a GaN substrate is used (for Ga-rich devices). In order to correctly simulate and predict waveguiding the refractive indices of all involved layers need to be known. Typically, the bulk refractive indices derived using Sellmeier equation are used to estimate the difference in the refractive indices between the cladding and waveguiding layers [64, 65, 198]. Since the difference of the Al content between these two layers is often rather small (10–20%), the resulting Δn is in the range of 0.05 to 0.1, which limits the waveguiding efficiency and decreases the confinement for the laser mode. Approaches to improve the confinement of the laser light in the waveguide include the use of a graded layers for polarization doping, which helps in the confinement by providing a higher effective refractive index and in addition avoids Mg doping related losses. This approach is similar to that used in visible lasers (GRINSCH) and has been a critical part of the first UVC laser diode [8].

Experimentally, the effective refractive index of the optical mode is accessible by observing cavity modes in optically pumped laser diodes [63, 199]. Figure 8 shows cavity modes recorded around the laser threshold from lasers emitting at 265 nm and 271 nm. Both MQWs were exhibiting a comparable laser threshold and were grown on undoped and n-type AlGaN waveguiding layers, respectively. The latter result is significant as it proves that n-doping of the optical confinement layers does not introduce additional absorption or refractive index change that would detrimentally influence the gain.

The longitudinal modes are equally spaced and the effective refractive index of the cavity can be obtained by the Fabry–Perot etalon equation. If the cavity length is d, for a given wavelength (λ) the distance between two neighboring longitudinal modes is given by:

$$\Delta\lambda = \frac{\Delta m\lambda^2}{2d(n_{\mathrm{eff}} - \lambda\frac{dn_{\mathrm{eff}}}{d\lambda})} \approx \frac{\lambda^2}{2dn_{\mathrm{eff}}}$$

where n_{eff} is the corresponding effective refractive index of the waveguide (depending on the wavelength—Fig. 9—left) [63]. In Fig. 9 (left), cavity modes for two different cavity lengths (120 µm and 290 µm) are shown. As expected, and following the above equation, the mode separation increases for shorter cavity length. Figure 9 (left) shows the mode separation for a variety of laser cavity lengths (red and black dots). The curve was fitted using the above equation and a refractive index of 3.5 was calculated. This is much higher than the refractive index of bulk AlGaN ($n = 2.4$) obtained by the ellipsometry measurements [64].

With these updated refractive indices, the confinement factors can be calculated. It is found that in optically pumped

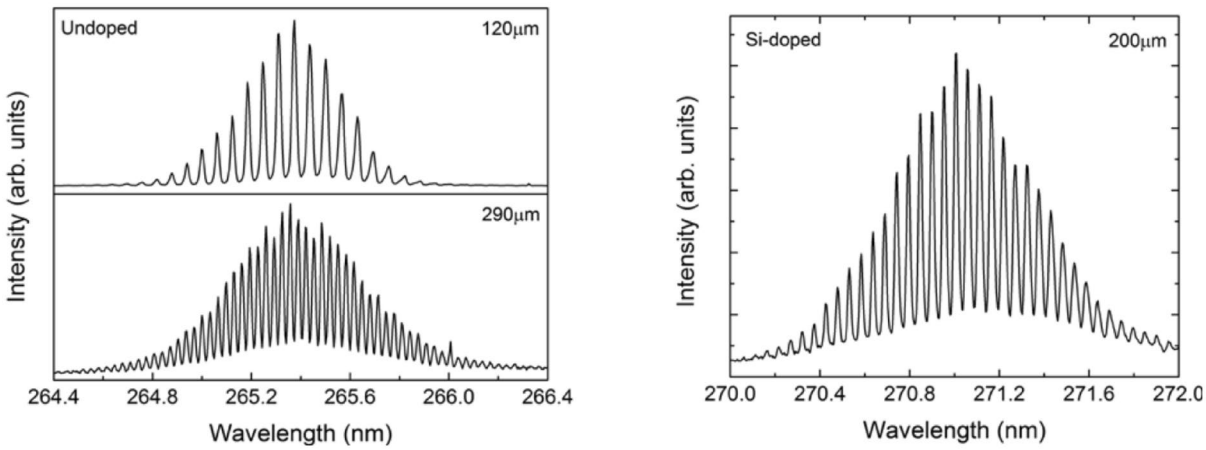

Figure 8: (left) Experimentally observed cavity modes from a mid-UV laser emitting at 265 nm for two different cavity lengths. The structure consisted of 11 MQWs with 4 nm AlN barriers and 2 nm 55% AlGaN wells. As expected, the separation between the cavity modes changes with cavity length (120 μm vs. 290 μm). This allows for a calculation of the effective refractive index of the waveguide, which is otherwise practically impossible to measure. (right) Cavity modes were also observed for doped waveguides and no influence of Si-doping on the refractive index or absorption was found.

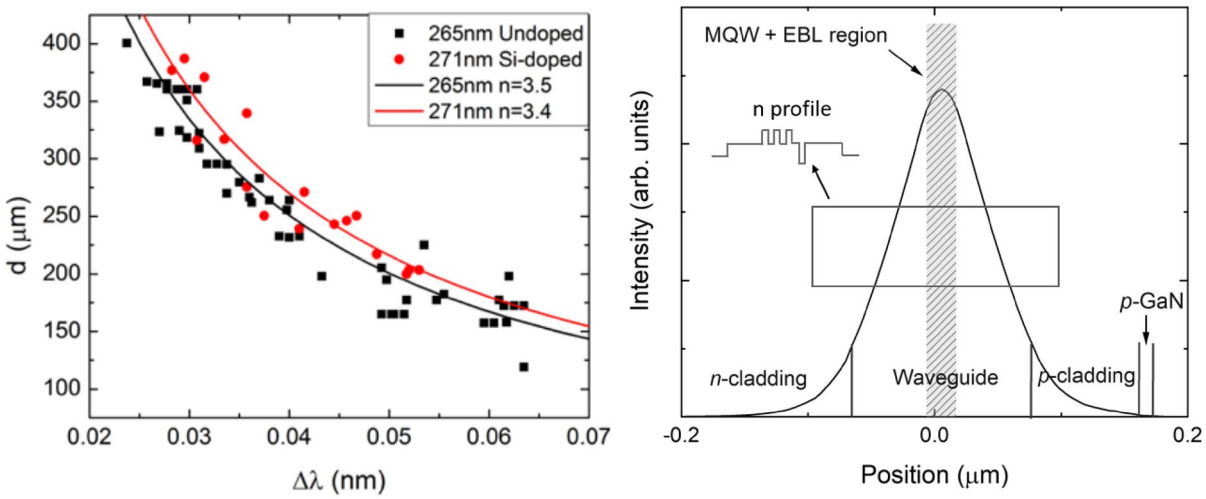

Figure 9: (left) Cavity length of two lasers emitting at 265 nm (black) and 271 nm (red) as a function of the mode spacing. The laser emitting at 271 nm was grown on an n-type AlGaN cladding layer. The dots indicate the experimentally determined mode spacing of different lasers and lines are best fits to the measurements. The calculated refractive indices are 3.4 and 3.5 for the two wavelengths, respectively. (right) Light intensity distribution for an electrically injected UVC laser diode based on Silvaco simulation. The refractive index profile is indicated in the figure. For the simulation a non-absorbing AlN substrate was assumed.

structures with the MQWs (targeted emission 270 nm) sitting on top of 500-nm-thick AlGaN layers (70% Al content), most of the light will travel in the AlGaN and not the MQW. Using the definition of the confinement factor Γ as the overlap between the gain medium and the optical mode, it was found that for such an optically pumped laser with no effective waveguide, Γ can be as small as 1% or even less [67, 200]. A reduction of the AlGaN layer thickness from 500 to 100 nm in optically pumped lasers results in $\Gamma \approx 2\%$.

Naturally, for real lasers, the MQW would be embedded in two AlGaN layers forming the actual waveguide (embedded in the cladding layers). Simulations suggest that for symmetrical waveguides with the MQW embedded in a 200 nm $Al_{0.7}Ga_{0.3}N$ (50 nm p-type + 50 nm n-type AlGaN) layer, grown on a n-type $Al_{0.8}Ga_{0.2}N$ cladding layer, more than 95% of the mode is confined in the waveguide (Fig. 9—right). For an active region of 20 nm thickness a confinement factor of $\Gamma > 5\%$ is found which is comparable to that of InGaN laser diodes [63, 201].

Having as much of the UV light confined in the waveguide and preventing leakage into the cladding layers is of utmost importance in UV lasers. As discussed above, UV laser diodes typically use thin GaN contact layers for hole injection

which are, similar to the Ni/Au contacts, absorbing for light emitted below 350 nm (above bandgap absorption results in $\alpha > 100{,}000\ cm^{-1}$). If enough of the UV laser light wave penetrates the p-GaN contact layer the threshold is significantly increased or the laser may not show lasing at all because it cannot sustain the high absorption loss. As a rule of thumb, considering band edge absorption coefficients, it can be predicted that if less than 0.05% of the optical wave travels in the absorbing p-GaN (or Ga-rich AlGaN in polarization doped AlGaN) the loss should be comparable to maximum achievable gain of the active region. The simulation in Fig. 9 (right) does include a p-GaN contact layer. However, due to the thickness of the p-AlGaN cladding layer and the low thickness of the p-GaN contact layer (20–40 nm), the confinement factor is only slightly impacted compared to a device without p-GaN; if designed correctly the p-GaN losses can be avoided. It is found that for reasonable layer thicknesses the threshold for electrically injected lasing can be kept at achievable values, but it is pointed out that it strongly depends on cladding thickness, particular Al contents, and GaN thickness [59, 63].

Figure 10 shows simulation results for the laser threshold as a function of optical loss in a laser structure consisting of a n-cladding layer (500 nm, 75% Al), n-waveguide (60 nm, 65% Al), 3xMQW (AlGaN/AlGaN, 3 nm/3 nm), electron blocking layer (EBL, 10 nm, 80% Al), p-waveguide (60 nm, 65% Al), p-cladding (75% Al), and a p-GaN contact layer (20 nm) [60]. The optical loss for different cladding thicknesses is indicated in Fig. 10 as well. The data only considers loss in p-GaN due to the cladding layer thickness, other losses such as those related to defect absorption centers, facet losses, or scattering losses are not considered. It is found that for a 500-nm-thick p-cladding layer the calculated loss is on the order of 5 cm^{-1}, which reduces the expected threshold to about 2 kA/cm^2, which is close to the value needed to achieve population inversion in the MQWs. A reduction of the thickness increases the loss non-linearly and for cladding layer thickness < 60 nm the absorption loss becomes so dominant that lasing cannot be achieved as the required threshold currents are prohibitively high. Choosing the desired p-cladding thickness needs to consider these losses and in addition the electrical properties of the laser device. Since the doping efficiency of AlGaN:Mg is very low due to compensation and high activation energy of the acceptor, the p-AlGaN cladding layer has a very high series resistance. Too thick of a p-AlGaN layer is not favorable for hole transport which makes thinner cladding layer more favorable. However, since the optical loss increases so significantly with decreasing p-AlGaN thickness, a 500-nm-thick cladding layer is suggested for a 270 nm laser structure to reduce absorption from p-GaN layer. Similar p-cladding thicknesses are incorporated in UV laser grown on absorbing GaN substrates and were successfully used to achieve UVA lasing [121, 194, 198].

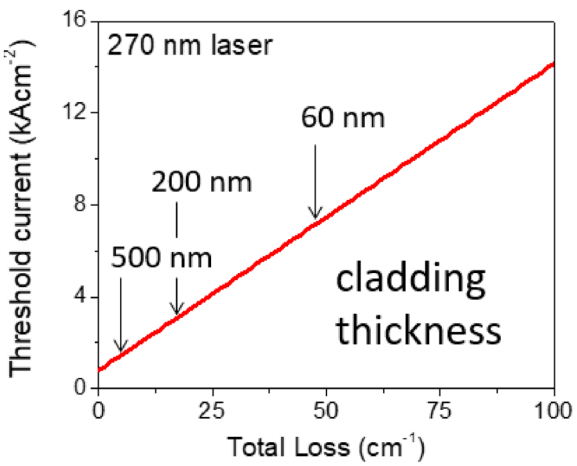

Figure 10: Simulation results for the threshold current as a function of optical loss in the laser diode. The loss in p-GaN for different p-cladding layer thickness is indicated. For thin p-cladding layers a higher loss and therefore a higher threshold are expected.

Improving the efficiency of MQWs

The active region of a laser diode is the MQW structure. It is difficult to assess how a MQW will perform in a laser diode without having a working device. Given the few demonstrations of AlGaN-based lasers in the UVB and UVC, the internal quantum efficiency (IQE) and the laser threshold in optically pumped devices are typically used to provide at least some guidance. However, both values are never to be understood as absolute and are rarely even comparable from one group to another due to the difficulties in the experimental setup and challenges in the calibration. This is especially true for the laser threshold measurement, where estimating the actual power density is rather challenging (with the spot size being the highest contributor to the error). A more reliable benchmark for AlGaN-based MQWs is the IQE, which can be calculated using either room temperature/low temperature relative intensity measurements or by integrated PL intensity as a function of excitation power using the Shockley–Read–Hall (SRH) model. The first is a quick and commonly utilized method, however, it assumes 100% efficiency at low temperature which may not be reasonable at all times [38, 202]. In the SRH model, the recombination rate (neglecting Auger recombination) is given by:

$$G = An + Bn^2$$

where n is the carrier density, A is the non-radiative coefficient and B is the radiative coefficient.

Previously, temperature-dependent and power-dependent IQE measurements both produced similar IQE values in AlGaN-based MQWs, allowing the use of the SRH model

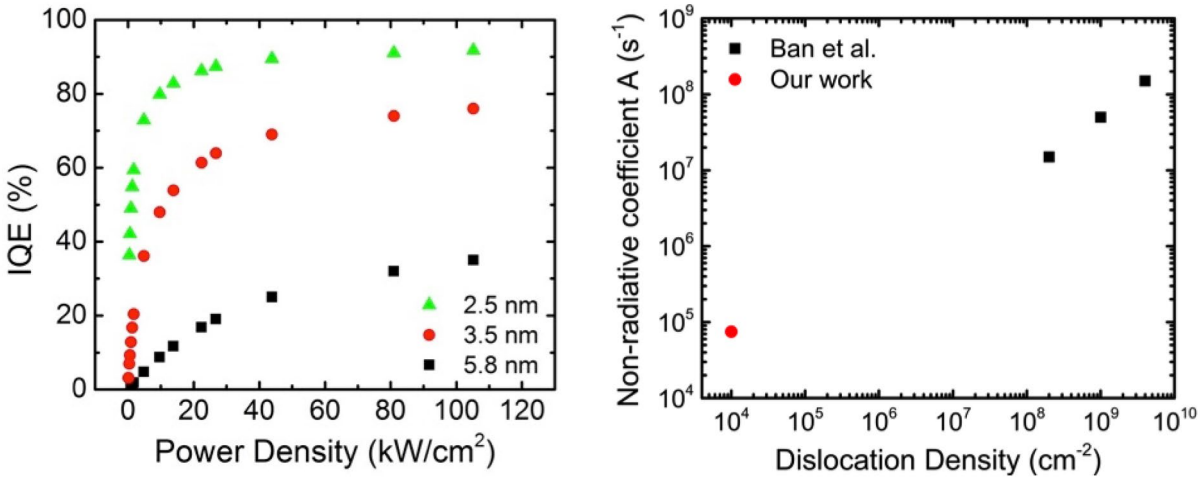

Figure 11: (left) Power-dependent IQE of $Al_{0.75}Ga_{0.25}$ N/AlN quantum well structures grown on AlN for different quantum well thicknesses. A decrease in quantum well thickness increases the IQE significantly. Thin quantum wells as they were used in our initial experiments are beneficial for high IQE and consequently low threshold and high gain. For the thinnest MQW structures a record IQE exceeding 90% was demonstrated for relatively low pumping powers. (right) Non-radiative coefficient (A) as a function of dislocation density for MQW structures grown on different substrates [37, 46].

to determine the A coefficients. Auger recombination in AlGaN-based devices is typically neglected due to the wide bandgap of the material and experimental findings, however, recent findings indicate that under certain circumstances it has to be included [202]. Figure 11 (left) shows the IQE for $Al_{0.75}Ga_{0.25}$ N/AlN MQWs as a function of the optical pumping power. Here, a strong dependence on the well width is observed. This is related the impact of the quantum confined Stark effect [51, 203]. IQE close to 100% was observed for devices grown on native substrate, which is enabled by the low dislocation density in the active region [37]. This by a factor of 2–3 higher than the best IQEs reported on sapphire substrates [77, 204].

In addition to the dislocation density, the growth conditions during the MQW growth and with it the incorporation of point defects, was found to be a crucial factor that impact the IQE of AlGaN-based MQWs [38, 46, 205]. For example Bryan et al. showed that with an increase in the V/III ratio by a factor of 10, which resulted in the reduction of impurities and other native point defects, the IQE increased from 57 to 91% [46]. These high IQE values where achieved at relatively low excitation power densities around 20 kW/cm^2, corresponding to carrier densities around 10^{18} cm^{-3}, which is below the carrier densities required to achieve population inversion for lasing. The high IQE is a direct result of decreasing the non-radiative (A) coefficient to the values below 10^5 s^{-1}. Figure 11 (right) shows a comparison between the non-radiative (A) coefficients obtained from best structures grown by Ban et al. on sapphire and by Bryan et al. on AlN substrates [37, 46]. Both the decrease in non-radiative coefficient and improvement in IQE with an increase in V/III ratio in these low dislocation density structures indicate the importance of dislocation and point defect management and their role in non-radiative recombination.

Another important factor for the performance of UV laser active regions is the optical gain. A positive net gain is a necessity to achieve either optically- or electrically pumped lasing. The gain achieved in the active region must overcome any other losses as discussed above. Achieving high gain is therefore of utmost importance since it is a direct measure of material's potential for light amplification. The materials gain of most III-nitrides, including AlGaN, can be as high as 4000 cm^{-1} [206, 207]. However, the modal gain typically has much lower values since it's given by the overlap of the optical wave and the active region (MQW), the Γ-factor. Given typical thicknesses of the MQW (20–40 nm) and the waveguide (100–200 nm), one can expect Γ-factors up to ~ 7%, resulting in peak modal gain of < 100 cm^{-1} [63, 208].

Most gain studies in AlGaN were made using the Variable-Stripe-Length (VSL) method. Alternatively, Hakki–Paoli method and segmented contact technique were used [209, 210]. The VSL method allows for the measurement of the net optical gain and gain threshold in the entire UVC range. The relation between the intensity of the emitted light and the stripe length is described as:

$$I_{ASE}(l,\lambda) = \frac{\alpha}{G(\lambda)}\left(e^{G(\lambda)*l} - 1\right)$$

where $I_{ASE}(l,\lambda)$ is the amplified spontaneous emission intensity, α is a constant related to the spontaneous emission, G is the net optical gain, and l is the stripe length [206]. Figure 12 shows modal gain spectra under different pumping power densities for a MQW structure emitting at ~ 260 nm. The laser threshold

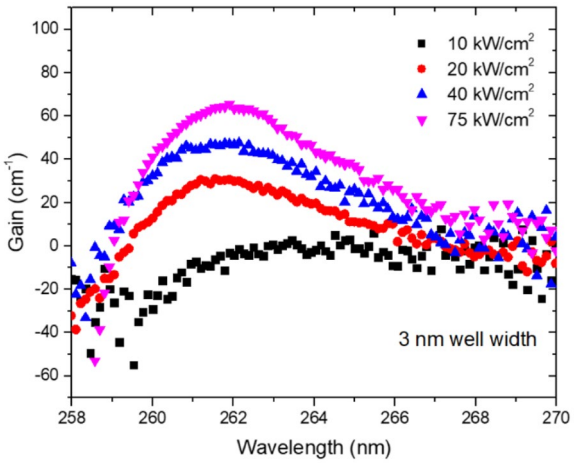

Figure 12: Gain as a function of the wavelength obtained from VSL method.

pumping power density for this structure was around 10 kW/cm^2 and the measured modal gain values as high as 60 cm^{-1} were obtained.

The actual peak modal gain of a MQW structure will strongly depend on the MQW design including well width, barrier width, composition, etc. Furthermore, any point defects or extended defects that lead to an absorption of the targeted wavelength will further reduce the achievable peak gain. Experimental and theoretical work from Guo et al. showed that for electrically injected structures with targeted emission around 265 nm, a 3 × MQW with 2 nm well and 6 nm barrier width may be beneficial [67]. These numbers are close to those values of MQWs typically employed in UVC LEDs. This finding was further confirmed by a recent work from Witzigmann et al. who claimed that maximum gain may be achieved in MQWs with well width of 2.2 nm [208]. Interestingly enough, they also found that a comparable gain may be achieved in single quantum wells with width exceeding 6 nm. The latter is exactly the strategy employed by Zhang et al. to achieve electrically injected lasing [8]. The advantage of SQWs over MQWs is the potential to achieve population inversion at lower currents and thus lasing at lower current densities. However, this is only true for low loss devices (including mirror losses, absorption, etc.).

The reported peak modal gain values of optimized AlGaN-based MQWs are typically comparable and around 50–80 cm^{-1} [206, 207, 211, 212]. This is despite using different substrates (sapphire, AlN), having different MQW designs, and having different epitaxial layer quality. While this may be initially surprising it is pointed out that these peak gain values are achieved at vastly different pumping power densities ranging from just a few kW/cm^2 to MW/cm^2, which is in agreement with reported optically pumped laser thresholds. In other words, while most MQWs can achieve peak gain values that are reasonably high, they do so at orders of magnitude different carrier densities.

The reported peak gain values of UV emitting MQWs are comparable to those in InGaN emitting in the visible part of the spectrum. For example, Nakamura et al. reported in one of the first InGaN-based MQWs for blue laser diodes peak gain values of 110 cm^{-1} and intrinsic losses of 60 cm^{-1} [34, 213]. Such gain values were found to be reasonable for electrically injected laser diodes, which highlights that this is also be achievable in the UV range if sufficient and stable carrier injection can be achieved in AlGaN-based devices. Lastly, a potential pathway to increase the IQE further was recently highlighted by Murotani et al. [214] They found that temperature dependence of the threshold excitation power density suggested that the mechanism of optical gain formation changed from excitonic transition to degenerated electron–hole plasma between 200 and 250 K. Fostering room temperature, excitonic-driven recombination should reduce the threshold of UV laser diodes below the already demonstrated numbers, however, the underlying methods to control this as still unknown and need further exploration.

Innovations in electron blocking layer design

In semiconductors, the electrons in the conduction band typically exhibit a much lower effective mass relative to the holes in the valence band. For example, in GaN, the effective mass of electrons is 0.2 and that of "heavy" holes is 2 [215]. Consequently, the electron mobility is typically an order of magnitude higher than the hole mobility, resulting in an excess electron current in the GaN/InGaN-based laser p–n diode in addition to electron–hole recombination current thus greatly lowering the injection efficiency. As a solution, in GaN/InGaN-based laser diodes, an electron blocking layer consisting of AlGaN with an appropriate Al composition ensuring bandgap sufficiently larger than GaN is employed. This has ensured high efficiency emitters in the UVA and VIS range. However, AlGaN presents a more interesting challenge. The mobility of holes in Al-rich AlGaN is expected to be much lower than in p-GaN as evidenced by the resistivity of p-AlGaN being approximately two orders of magnitude higher than p-GaN even with a lower activation energy [54]. Consequently, the asymmetry between the electron and hole conduction is much larger in Al-rich AlGaN and the associated losses are expected to be much larger in deep-UV emitters. This issue is further exacerbated by the requirement of thick p-AlGaN cladding to reduce absorption losses in p-GaN employed as hole injection layer and p-contact layer. Among the challenges is that the conduction band offset even with AlN EBL isn't sufficient to prevent electron overshoot [180] with the likely side-effect of presenting a hole barrier as well. Consequently,

EBL design has been actively researched for improved charge injection efficiency. As a notable advancement in this direction, multiple quantum barrier electron blocking layer (MQB-EBL) has been demonstrated to improve the external quantum efficiency in deep-UV (250 nm) LEDs by a factor of 3 where the AlGaN/AlGaN superlattice-based EBL is expected to act as a better electron barrier by multiple reflections of the electron wavefunction, while allowing for sufficient thermal emission of holes across the superlattice [180]. Nonetheless, despite the novel approaches and the potential to use results from UV LEDs, optimization of EBLs for laser diodes will need to be addressed in the future to reduce thresholds.

Optical losses and distributed Bragg reflectors

Optical losses in AlGaN-based UV laser diodes have already been discussed above. If not taken care of, one of the biggest losses can be absorption in the p-GaN contact layer and at the p-contact (if employed as hole injection layer). However, this loss can be managed by designing the p-cladding layer correctly and by reducing the p-GaN thickness as much as possible. Other losses include (a) loss in p-type (Mg-doped) AlGaN waveguide and cladding, (b) mode leakage to the n-side (through impurities and substrate leakage), and (c) optical loss at the facets.

P-AlGaN-related absorption loss has been reported to be substantial (50 cm^{-1}) [47]. In visible laser diodes, the p-side is often not doped at all or has a reduced p-doping level. An illustration of the loss related to p-AlGaN is shown in Fig. 13.

For devices emitting in the 265 nm range, different waveguide configurations were investigated. It was found that for symmetric and asymmetric doping, as well as inclusion of Si-doping, the optically pumped laser threshold was impacted only negligibly (Sample 1–3). However, Mg doping of on one part of the waveguide (mode confinement < 50%) resulted in orders of magnitude higher laser threshold.

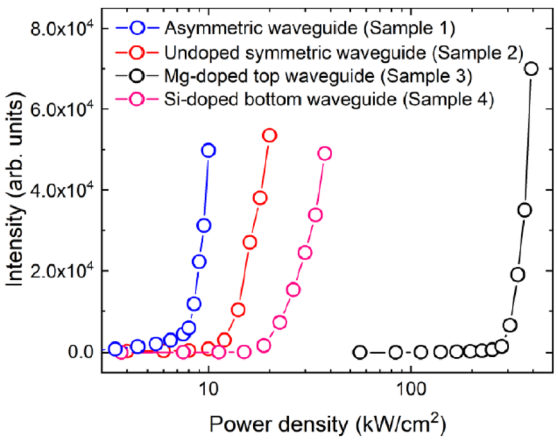

Figure 13: Threshold power values of the four optically pumped laser samples for different waveguide configurations. Sample 1 has an asymmetric waveguide (100 nm AlGaN/ MQW) and sample 2–4 have symmetric waveguides (50 nm AlGaN/MQW/50 nm AlGaN) but different doping configurations. All samples were grown on AlN substrates [from Ref. 51].

For visible lasers grown on native GaN substrates and with AlGaN cladding and/or waveguiding layers, mode leakage into the n-side is a major concern (since GaN effectively traps light due to its high refractive index) and is addressed by using hybrid InGaN/GaN waveguides [201, 216]. This may also be a major obstacle for UVB laser diodes grown on native GaN substrates (here the UV light is even absorbed), especially if the n-cladding is not thick enough. Devices grown on sapphire do not suffer from the same challenge due to the lower refractive index of sapphire compared to GaN and AlGaN. The same principle applies for UVC lasers grown on AlN single crystal substrates. This agrees well with theoretical data (e.g., Fig. 9–right), thus, for native AlN substrates n-side leakage is not considered a challenge (except if the cladding layer is defect-rich and provides for absorption losses).

Finally, due to the relatively low refractive index in ultra-wide bandgap Al-rich AlGaN, the mirror losses are also relatively high. Consequently, high threshold current densities are expected in these deep-UV laser diodes and may be prohibitively high. An important technology that may be employed to greatly lower the mirror loss and thereby reduce the threshold current is that of Distributed Bragg Reflectors (DBRs). Deposition of such DBRs on the facets of laser diodes can reduce the laser threshold of electrically injected devices. It was demonstrated that highly reflective mirrors with low absorption can be achieved with sputtered HfO_2/SiO_2 (99%) or YSZ/SiO_2 (99.9%) [217]. Compared to ~ 20% reflection at AlGaN facets, this represents a reduction in mirror loss from ~ 15 cm^{-1} for AlGaN facet exposed to air (cavity length of 1 mm) to 0.1 cm^{-1} and 0.01 cm^{-1} for facets coated with sputtered HfO_2/SiO_2 (99%) or YSZ/SiO_2 (99.9%), respectively. Hence a significant reduction in laser threshold current is expected. Accordingly, employing DBRs of HfO_2/SiO_2, Kao et al. demonstrated a reduction in laser threshold from 250 to 180 $kWcm^{-2}$ and the first electrically injected UVC laser also employed DBRs [218, 219]. For the latter, DBRs were deposited in-situ using ALD on etched facets that limits the number of pairs and hence the reflectivity, and the advantage of high reflectivity sputtered DBRs on cleaved facets is to be exploited in the future.

Optically and electrically induced UV lasing

Electrically injected (pulsed) UV lasing based on AlGaN technology has been demonstrated in the UVB and UVC range down to 260 nm, however, the commercially available shortest wavelength is still based on InGaN and emitting around 380 nm. Generally, the achieved electrically pumped laser diodes can

be subdivided in three groups: (a) laser diodes emitting in the 340–350 nm range, and (b) diodes emitting below 340 nm but still UVA, and (c) UVB and UVC lasers. The first group utilizes efforts from InGaN laser growth: Low Al content AlGaN layers with high doping capabilities can be grown on sapphire substrates using the same growth and fabrication routine employed for InGaN lasers. Typical thresholds for these laser diodes are in the single digit kA/cm^2 range and output powers as high as a few tenth of mW have been demonstrated [4, 194, 220–222]. While almost all of these diodes were grown on non-native substrates, they all benefit from low dislocation templates or ELO technology with dislocation densities in the 10^8 cm^{-2} range, which is in agreement with laser diodes in the visible wavelength range.

The second group of laser diodes is based on mid-range Al contents. For these devices, InGaN technology is not helpful anymore and special efforts to achieve thick AlGaN layers and doping must be made. Most devices in the 320–330 nm (UVA) wavelength range have been demonstrated by Hamamatsu and their collaborators. These devices were grown on sapphire and GaN substrates and relied on facet controlled epitaxial lateral overgrowth (FACELO) substrates [223, 224]. Using FACELO, dislocation density reduction and relaxation of AlGaN with 30–40% Al content is possible, which in turn allows the growth of laser structures with relatively low dislocation densities. Using this technology, lasing down to about 320 nm has been demonstrated and output power of up to 1 W was achieved [194, 225]. However, the threshold current density was typically in the 10–40 kA/cm^2 range, indicating significant losses and significant heating, which in turn limits the lifetime of the devices. Interestingly enough, the device performance does not improve when the FACELO technology was applied on GaN substrates instead of GaN/sapphire substrates, indicating that the relaxation of AlGaN on GaN is still challenging [121].

UVB and UVC emitters are rather new. The first electrically injected UVC laser diode was based on nanowires and self-aligned cavities [7, 226]. For the UVC wavelength range, it is suspected that lasing in these nanowire lasers was achieved by a decreased defect density and increased conductivity due to the small feature size of the active region. Self-aligned cavities were then formed and emission at 262 nm was observed. Operation temperature seemed to be limited to 77 K due to the maximum achievable gain, related to very large inhomogeneous broadening associated with the 3D compositional variations in randomly formed AlGaN nanowire arrays.

More recent UVB and UVC lasers rely on more traditional approaches. Sato et al. presented operation of an AlGaN-based UVB laser diode emitting at 298 nm and operating at room temperature [227]. Growth was done on relaxed AlGaN/AlN/sapphire substrates with assumed dislocation density of 10^8 cm^{-2}. Depending on the device configuration, laser threshold current densities between 40 and 70 kA/cm^2 and operating

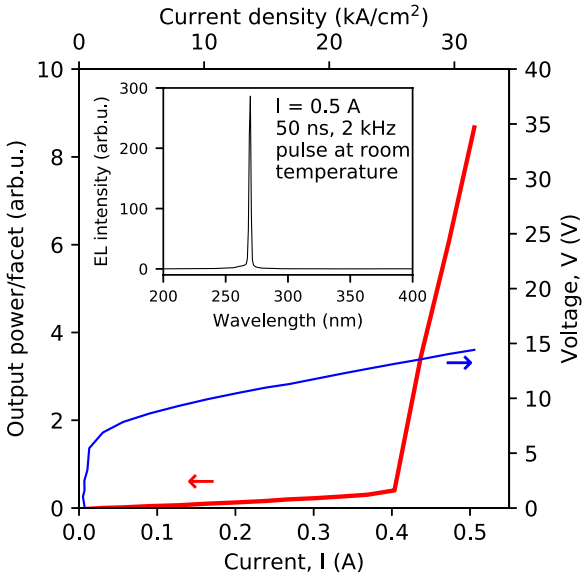

Figure 14: I–V and I–L curve of an edge emitting diode with peak emission around 280 nm [from Ref. 8].

voltages around 30 V were needed, resulting in limitation to pulsed operation and low output power (≈ 0.3 mW). The first edge emitting laser diode operating in the UVC range was demonstrated by Zhang et al. [8] This diode was grown on native AlN substrates to reduce the dislocation density below 10^5 cm^{-2}. Emission wavelength was between 270 and 280 nm and output power was in the single digit mW range (Fig. 14).

The UVC laser diode had a lower threshold and operating voltage compared to the UVB laser from Sato et al. This resulted in a 4–6 times lower electrical power needed to operate the device. Nonetheless, the operation was limited to pulsed operation with a duty cycle of 0.02%. Achieving of UVC lasing at these relatively good values is likely related to a few unique innovations that were included in this device: (a) the use of a low dislocation AlN substrate, (b) implementation of an undoped graded layer on the p-cladding side, (c) use of a 9-nm-thick single quantum well compared to the more commonly used MQWs, (d) deposition of oxide-based DBRs on etched facets, and (d) fabrication of relatively short cavities (400 μm) with 4 μm wide injection areas (p-contact).

Apart from electrically injected lasing, optically pumped lasing has been demonstrated more commonly over the whole UVB and UVC range. The shortest wavelength stimulated emission (not lasing) was achieved from pure AlN structures at 216 nm with threshold optical power density of approximately 9 MW/cm^2 [228]. For MQW structures and other confined structures the early work focused on the Ga-rich side and UVA [229, 230]. The first UVC optically pumped lasing using MQWs was achieved by Takano at 240 nm [231]. The initial threshold pumping power was approximately 1200 kW/cm^2 at room temperature and the laser was grown on a 4H-SiC substrate.

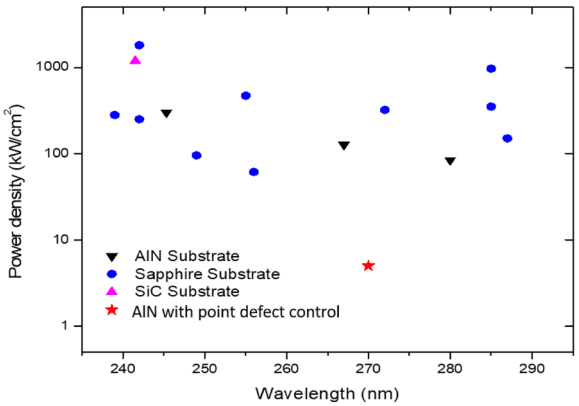

Figure 15: UVC laser threshold of optically pumped lasers achieved by different groups [38, 199, 218, 232–235].

Since then, optically pumped lasing has been demonstrated on many different substrates and templates. Again, and as shown in Fig. 15, a general trend toward lower threshold for laser grown on lower dislocation templates is observed. However, it was also shown that point defects and impurity density have a significant impact on the optical laser threshold [38]. Therefore, for both optically and electrically pumped laser diodes, it is of utmost importance to control and reduce extended and point defects.

Outlook

While the early works on UV laser diodes started at the end of the last century, the main efforts were made only in the last ten years. This is a short range of time compared to any other effort for optoelectronic devices. Even GaAs laser diodes needed decades to mature before widespread commercialization was possible. Even though it may not be obvious, the advances that have been made in this field are tremendous and the outlook is positive. With the recently demonstrated lasers in the UVB and UVC range this outlook gets even brighter. The fact that optically pumped lasing can be achieved in UVC devices even on sapphire substrates indicates that the non-radiative recombination and losses of the waveguide cannot be too high to forbid lasing in the UV. It rather indicates that the electrical properties such as doping, contacts, and carrier injection need to be controlled and improved, which is where the main effort should be put in the years to come. While the first electrically injected laser in the UVC utilized polarization doping, this technology is still not fully understood. More investigations are needed to clarify the underlying mechanisms of this polarization doped layer especially with respect to band engineering and injection efficiency improvements. Thereby, traditional or mixed approached in designing UVB and UVC laser should not be neglected as they may offer more stability and ultimately lower threshold currents which in turn decrease heating and enable cw operation. By comparing the predicted laser threshold of UVB and UVC devices to theoretical values and those achieved in VIS laser, it is clear that the recent results are only a starting point and not the end.

It is clear that UV lasers based on AlGaN can only be made on substrates or templates with dislocation density in the low 10^8 cm^{-2} or below. Achieving these values consistently and with a high yield is mandatory for future commercialization efforts. Further efforts should be made to improve growth and fabrication of lasers. This includes such fundamental research as improvement of native AlN substrates and epitaxial growth on these substrates, development of low resistivity contacts to the p-side, and strengthening of the facet formation procedure and mirror deposition techniques. It is believed that at this point AlGaN-based lasers can greatly learn from efforts made for InGaN laser at the beginning of the century. For the coming years a steep learning curve is needed to finally allow for commercialization of UVC and UVB lasers, cw operation, and implementation of these devices on the system level.

Funding

The authors acknowledge funding in part from AFOSR (Nos. FA9550-17-1-0225, FA9550-19-1-0114, and FA9550-19-1-0358), the National Science Foundation (Nos. ECCS-1508854, ECCS-1610992, ECCS-1916800, and ECCS-1653383), and ARO (No. W911NF-16-C-0101).

Declarations

Conflict of interest On behalf of all authors, the corresponding author states that there is no conflict of interest.

References

1. R.N. Hall, G.E. Fenner, J.D. Kingsley, T.J. Soltys, R.O. Carlson, Phys. Rev. Lett. **9**, 366 (1962)
2. M.I. Nathan, W.P. Dumke, G. Burns, F.H. Dill Jr, G. Lasher, Appl. Phys. Lett. **1**, 62 (1962)
3. Z.I. Alferov, V. Andreev, D.Y. Garbuzov, Y. Zhilyaev, E. Morozov, E. Portnoi, V. Trofim, Sov. Phys. Semicond. **4**, 1573 (1971)
4. M. Kneissl, D.W. Treat, M. Teepe, N. Miyashita, N.M. Johnson, Appl. Phys. Lett. **82**, 2386 (2003)
5. Y. Enya, Y. Yoshizumi, T. Kyono, K. Akita, M. Ueno, M. Adachi, T. Sumitomo, S. Tokuyama, T. Ikegami, K. Katayama, T. Nakamura, Appl. Phys. Express **2**, 082101 (2009)
6. H. Yoshida, Y. Yamashita, M. Kuwabara, H. Kan, Appl. Phys. Lett. **93**, 241106 (2008)
7. S. Zhao, X. Liu, S.Y. Woo, J. Kang, G.A. Botton, Z. Mi, Appl. Phys. Lett. **107**, 043101 (2015)

8. Z. Zhang, M. Kushimoto, T. Sakai, N. Sugiyama, L.J. Schowalter, C. Sasaoka, H. Amano, Appl. Phys. Express **12**, 124003 (2019)
9. R. Collazo, S. Mita, J. Xie, A. Rice, J. Tweedie, R. Dalmau, Z. Sitar, Phys. Status Solidi C **8**, 2031 (2011)
10. S.A. Asher, Anal. Chem. **65**, 59A (1993)
11. E.V. Efremov, F. Ariese, C. Gooijer, Anal. Chim. Acta **606**, 119 (2008)
12. M. Gaft, L. Nagli, Opt. Mater. **30**, 1739 (2008)
13. M.A. Würtele, T. Kolbe, M. Lipsz, A. Külberg, M. Weyers, M. Kneissl, M. Jekel, Water Res. **45**, 1481 (2011)
14. L. Bachmann, D.M. Zezell, A.C. da Ribeiro, L. Gomes, A.S. Ito, Appl. Spectrosc. Rev. **41**, 575 (2006)
15. J.B. Irving, R.M. Judith, Phys. Med. Biol. **42**, 803 (1997)
16. S.T. Hess, S. Huang, A.A. Heikal, W.W. Webb, Biochemistry **41**, 697 (2002)
17. N. Hudson, A. Baker, D. Reynolds, River Res. Appl. **23**, 631 (2007)
18. D. Wan, H.-L. Chen, S.-C. Tseng, L.A. Wang, Y.-P. Chen, ACS Nano **4**, 165 (2010)
19. A.S. Matharu, S. Jeeva, P.S. Ramanujam, Chem. Soc. Rev. **36**, 1868 (2007)
20. B.J. Lin, J. Vac. Sci. Technol. **12**, 1317 (1975)
21. Z. Xu, B.M. Sadler, IEEE Commun. Mag. **46**, 67 (2008)
22. G. Chen, L. Liao, Z. Li, R.J. Drost, B.M. Sadler, (2014), pp. 904–909
23. R. Torsten, D. Ralph, Laser Technol. J. **6**, 20 (2009)
24. H. Häffner, C.F. Roos, R. Blatt, Phys. Rep. **469**, 155 (2008)
25. R. Islam, E.E. Edwards, K. Kim, S. Korenblit, C. Noh, H. Carmichael, G.D. Lin, L.M. Duan, C.C. Joseph-Wang, J.K. Freericks, C. Monroe, Nat. Commun. **2**, 377 (2011)
26. T. Makimura, S. Mitani, Y. Kenmotsu, K. Murakami, M. Mori, K. Kondo, Appl. Phys. Lett. **85**, 1274 (2004)
27. S. Mishra, V. Yadava, Opt. Lasers Eng. **73**, 89 (2015)
28. K.-R. Kim, J.-H. Cho, N.-Y. Lee, H.-J. Kim, S.-H. Cho, H.-J. Park, B. Choi, J. Manuf. Syst. **38**, 107 (2016)
29. U. Kogelschatz, H. Esrom, J.Y. Zhang, I.W. Boyd, Appl. Surf. Sci. **168**, 29 (2000)
30. J.J. McFerran, L. Yi, S. Mejri, S. Di Manno, W. Zhang, J. Guéna, Y. Le Coq, S. Bize, Phys. Rev. Lett. **108**, 183004 (2012)
31. W.H. Oskay, S.A. Diddams, E.A. Donley, T.M. Fortier, T.P. Heavner, L. Hollberg, W.M. Itano, S.R. Jefferts, M.J. Delaney, K. Kim, F. Levi, T.E. Parker, J.C. Bergquist, Phys. Rev. Lett. **97**, 020801 (2006)
32. T.-J. Lu, M. Fanto, H. Choi, P. Thomas, J. Steidle, S. Mouradian, W. Kong, D. Zhu, H. Moon, K. Berggren, J. Kim, M. Soltani, S. Preble, D. Englund, Opt. Express **26**, 11147 (2018)
33. R. Dingle, C.H. Henry, (1976)
34. S. Nakamura, M. Senoh, S. Nagahama, N. Iwasa, T. Yamada, T. Matsushita, Y. Sugimoto, H. Kiyoku, Appl. Phys. Lett. **69**, 1568 (1996)
35. S. Nakamura, M. Senoh, S. Nagahama, N. Iwasa, T. Yamada, T. Matsushita, Y. Sugimoto, H. Kiyoku, Appl. Phys. Lett. **69**, 4056 (1996)
36. S.D. Lester, F.A. Ponce, M.G. Craford, D.A. Steigerwald, Appl. Phys. Lett. **66**, 1249 (1995)
37. K. Ban, J. Yamamoto, K. Takeda, K. Ide, M. Iwaya, T. Takeuchi, S. Kamiyama, I. Akasaki, H. Amano, Appl. Phys. Express **4**, 052101 (2011)
38. R. Kirste, Q. Guo, J.H. Dycus, A. Franke, S. Mita, B. Sarkar, P. Reddy, J. LeBeau, M.R. Collazo, Z. Sitar, Appl. Phys. Express **11**, 082101 (2018)
39. P. Reddy, S. Washiyama, F. Kaess, R. Kirste, S. Mita, R. Collazo, Z. Sitar, J. Appl. Phys. **122**, 245702 (2017)
40. N.A. Fichtenbaum, T.E. Mates, S. Keller, S.P. DenBaars, U.K. Mishra, J. Cryst. Growth **310**, 1124 (2008)
41. F. Kaess, S. Mita, J. Xie, P. Reddy, A. Klump, L.H. Hernandez-Balderrama, S. Washiyama, A. Franke, R. Kirste, A. Hoffmann, R. Collazo, Z. Sitar, J. Appl. Phys. **120**, 105701 (2016)
42. C. Lund, S. Nakamura, S.P. DenBaars, U.K. Mishra, S. Keller, J. Cryst. Growth **464**, 127 (2017)
43. A. Saxler, D. Walker, P. Kung, X. Zhang, M. Razeghi, J. Solomon, W.C. Mitchel, H.R. Vydyanath, Appl. Phys. Lett. **71**, 3272 (1997)
44. T. Tanikawa, S. Kuboya, T. Matsuoka, Phys. Status Solidi B **254**, 1600751 (2017)
45. P. Reddy, M.P. Hoffmann, F. Kaess, Z. Bryan, I. Bryan, M. Bobea, A. Klump, J. Tweedie, R. Kirste, S. Mita, M. Gerhold, R. Collazo, Z. Sitar, J. Appl. Phys. **120**, 185704 (2016)
46. Z. Bryan, I. Bryan, J. Xie, S. Mita, Z. Sitar, R. Collazo, Appl. Phys. Lett. **106**, 142107 (2015)
47. M. Martens, C. Kuhn, T. Simoneit, S. Hagedorn, A. Knauer, T. Wernicke, M. Weyers, M. Kneissl, Appl. Phys. Lett. **110**, 081103 (2017)
48. Z. Zhang, M. Kushimoto, M. Horita, N. Sugiyama, L.J. Schowalter, C. Sasaoka, H. Amano, Appl. Phys. Lett. **117**, 152104 (2020)
49. R. Collazo, J. Xie, B.E. Gaddy, Z. Bryan, R. Kirste, M. Hoffmann, R. Dalmau, B. Moody, Y. Kumagai, T. Nagashima, Y. Kubota, T. Kinoshita, A. Koukitu, D.L. Irving, Z. Sitar, Appl. Phys. Lett. **100**, 191914 (2012)
50. B.E. Gaddy, Z. Bryan, I. Bryan, J. Xie, R. Dalmau, B. Moody, Y. Kumagai, T. Nagashima, Y. Kubota, T. Kinoshita, A. Koukitu, R. Kirste, Z. Sitar, R. Collazo, D.L. Irving, Appl. Phys. Lett. **104**, 202106 (2014)
51. Q. Guo, *Engineering of Electrically Injected AlGaN-Based UVC Lasers* (North Carolina State University, Raleigh, 2019)
52. S. Nakamura, T. Mukai, M. Senoh, N. Iwasa, Jpn. J. Appl. Phys. **31**, L139 (1992)
53. B. Sarkar, S. Mita, P. Reddy, A. Klump, F. Kaess, J. Tweedie, I. Bryan, Z. Bryan, R. Kirste, E. Kohn, R. Collazo, Z. Sitar, Appl. Phys. Lett. **111**, 032109 (2017)
54. T. Kinoshita, T. Obata, H. Yanagi, S. Inoue, Appl. Phys. Lett. **102**, 012105 (2013)

55. J. Simon, V. Protasenko, C. Lian, H. Xing, D. Jena, Science **327**, 60 (2010)
56. P. Reddy, I. Bryan, Z. Bryan, J. Tweedie, S. Washiyama, R. Kirste, S. Mita, R. Collazo, Z. Sitar, Appl. Phys. Lett. **107**, 091603 (2015)
57. J.-S. Jang, K.-H. Park, H.-K. Jang, H.-G. Kim, S.-J. Park, J. Vac. Sci. Technol. B **16**, 3105 (1998)
58. B. Sarkar, P. Reddy, A. Klump, R. Rounds, M.R. Breckenridge, B.B. Haidet, S. Mita, R. Kirste, R. Collazo, Z. Sitar, in (2018), pp. 1–2
59. Z. Zhang, M. Kushimoto, T. Sakai, N. Sugiyama, L.J. Schowalter, C. Sasaoka, H. Amano, Jpn. J. Appl. Phys. **59**, 094001 (2020)
60. Q. Guo, R. Kirste, P. Reddy, S. Mita, R. Collazo, Z. Sitar, in (2018), pp. 1–4
61. T. Takano, T. Mino, J. Sakai, N. Noguchi, K. Tsubaki, H. Hirayama, Appl. Phys. Express **10**, 031002 (2017)
62. R. Kirste, S. Mita, P. Reddy, A. Franke, Q. Guo, K. Wang, R. Collazo, Z. Sitar, in (2019), pp. 1–3
63. Q. Guo, R. Kirste, P. Reddy, W. Mecouch, Y. Guan, S. Mita, S. Washiyama, J. Tweedie, Z. Sitar, R. Collazo, Jpn. J. Appl. Phys. **59**, 091001 (2020)
64. M. Rigler, M. Zgonik, M.P. Hoffmann, R. Kirste, M. Bobea, R. Collazo, Z. Sitar, S. Mita, M. Gerhold, Appl. Phys. Lett. **102**, 221106 (2013)
65. M. Rigler, J. Buh, M.P. Hoffmann, R. Kirste, M. Bobea, S. Mita, M.D. Gerhold, R. Collazo, Z. Sitar, M. Zgonik, Appl. Phys. Express **8**, 042603 (2015)
66. G.M. Laws, E.C. Larkins, I. Harrison, C. Molloy, D. Somerford, J. Appl. Phys. **89**, 1108 (2001)
67. Q. Guo, R. Kirste, S. Mita, J. Tweedie, P. Reddy, B. Moody, Y. Guan, S. Washiyama, A. Klump, Z. Sitar, R. Collazo, J. Appl. Phys. **126**, 223101 (2019)
68. Z. Bryan, I. Bryan, S. Mita, J. Tweedie, Z. Sitar, R. Collazo, Appl. Phys. Lett. **106**, 232101 (2015)
69. H. Kawanishi, M. Senuma, T. Nukui, Appl. Phys. Lett. **89**, 041126 (2006)
70. I. Bryan, Z. Bryan, S. Washiyama, P. Reddy, B. Gaddy, B. Sarkar, M. Hayden-Breckenridge, Q. Guo, M. Bobea, J. Tweedie, S. Mita, D. Irving, R. Collazo, Z. Sitar, Appl. Phys. Lett. **112**, 062102 (2018)
71. P. Bagheri, R. Kirste, P. Reddy, S. Washiyama, S. Mita, B. Sarkar, R. Collazo, Z. Sitar, Appl. Phys. Lett. **116**, 222102 (2020)
72. T. Kinoshita, T. Obata, T. Nagashima, H. Yanagi, B. Moody, S. Mita, S. Inoue, Y. Kumagai, A. Koukitu, Z. Sitar, Appl. Phys. Express **6**, 092103 (2013)
73. F. Mehnke, T. Wernicke, H. Pingel, C. Kuhn, C. Reich, V. Kueller, A. Knauer, M. Lapeyrade, M. Weyers, M. Kneissl, Appl. Phys. Lett. **103**, 212109 (2013)
74. B. Jacobs, M.C.J.C.M. Kramer, E.J. Geluk, F. Karouta, J. Cryst. Growth **241**, 15 (2002)
75. M. Lapeyrade, A. Muhin, S. Einfeldt, U. Zeimer, A. Mogilatenko, M. Weyers, M. Kneissl, Semicond. Sci. Technol. **28**, 125015 (2013)
76. A.A. Allerman, M.H. Crawford, A.J. Fischer, K.H.A. Bogart, S.R. Lee, D.M. Follstaedt, P.P. Provencio, D.D. Koleske, J. Cryst. Growth **272**, 227 (2004)
77. H. Hirayama, S. Fujikawa, N. Noguchi, J. Norimatsu, T. Takano, K. Tsubaki, N. Kamata, Phys. Stat. Sol. (a) **206**, 1176 (2009)
78. D. Liu, S.J. Cho, J. Park, J.-H. Seo, R. Dalmau, D. Zhao, K. Kim, J. Gong, M. Kim, I.-K. Lee, J.D. Albrecht, W. Zhou, B. Moody, Z. Ma, Appl. Phys. Lett. **112**, 081101 (2018)
79. H. Hirayama, N. Maeda, S. Fujikawa, S. Toyoda, N. Kamata, Jpn. J. Appl.Phys. **53**, 100209 (2014)
80. L. Liu, J.H. Edgar, Mater. Sci. Eng. R Rep. **37**, 61 (2002)
81. S. Iwama, K. Hayakawa, T. Arizumi, J. Cryst. Growth **56**, 265 (1982)
82. W.M. Yim, R.J. Paff, J. Appl. Phys. **45**, 1456 (1974)
83. R. Rounds, B. Sarkar, A. Klump, C. Hartmann, T. Nagashima, R. Kirste, A. Franke, M. Bickermann, Y. Kumagai, Z. Sitar, R. Collazo, Appl. Phys. Express **11**, 071001 (2018)
84. D.I. Florescu, V.M. Asnin, F.H. Pollak, A.M. Jones, J.C. Ramer, M.J. Schurman, I. Ferguson, Appl. Phys. Lett. **77**, 1464 (2000)
85. O. Lagerstedt, B. Monemar, Phys. Rev. B **19**, 3064 (1979)
86. R. Rounds, B. Sarkar, T. Sochacki, M. Bockowski, M. Imanishi, Y. Mori, R. Kirste, R. Collazo, Z. Sitar, J. Appl. Phys. **124**, 105106 (2018)
87. F. Briegleb, A. Geuther, Justus Liebigs Ann. Chem. **123**, 228 (1862)
88. G.A. Slack, T.F. McNelly, J. Cryst. Growth **34**, 263 (1976)
89. G.A. Slack, T.F. McNelly, J. Cryst. Growth **42**, 560 (1977)
90. C.M. Balkas, Z. Sitar, T. Zheleva, L. Bergman, I.K. Shmagin, J.F. Muth, R. Kolbas, R. Nemanich, R.F. Davis, MRS Proc. **449**, 41 (1996)
91. M. Bickermann, B.M. Epelbaum, O. Filip, P. Heimann, S. Nagata, A. Winnacker, Physica Status Solidi (c) **5**, 1502 (2008)
92. R. Schlesser, Z. Sitar, J. Cryst. Growth **234**, 349 (2002)
93. H. Helava, S.J. Davis, G.D. Huminic, M.G. Ramm, O.V. Avdeev, I.S. Barash, T.Y. Chemekova, E.N. Mokhov, S.S. Nagalyuk, A.D. Roenkov, A.S. Segal, Y.A. Vodakov, Y.N. Makarov, in *Physica Status Solidi C - Current Topics in Solid State Physics, Vol 4 No 7 2007* (Wiley-V C H Verlag Gmbh, Weinheim, 2007), pp. 2281–2284
94. V. Noveski, R. Schlesser, S. Mahajan, S. Beaudoin, Z. Sitar, J. Cryst. Growth **264**, 369 (2004)
95. J. Carlos Rojo, G.A. Slack, K. Morgan, B. Raghothamachar, M. Dudley, L.J. Schowalter, J. Cryst. Growth **231**, 317 (2001)
96. M. Tanaka, S. Nakahata, K. Sogabe, H. Nakata, M. Tobioka, Jpn. J. Appl. Phys. Part 2 **36**, 1062 (1997)
97. V. Noveski, R. Schlesser, B. Raghothamachar, M. Dudley, S. Mahajan, S. Beaudoin, Z. Sitar, J. Cryst. Growth **279**, 13 (2005)
98. M. Bockowski, M. Iwinska, M. Amilusik, M. Fijalkowski, B. Lucznik, T. Sochacki, Semicond. Sci. Technol. **31**, 093002 (2016)
99. S. Hagedorn, E. Richter, U. Zeimer, D. Prasai, W. John, M. Weyers, J. Cryst. Growth **353**, 129 (2012)

100. V. Sukhoveev, A. Usikov, O. Kovalenkov, V. Ivantsov, A. Syrkin, V. Dmitriev, C. Collins, M. Wraback, in *GaN, AIN, InN and Related Materials*. ed. by M. Kuball, T.H. Myers, J.M. Redwing, T. Mukai (Materials Research Society, Warrendale, 2006), pp. 743–748
101. K. Tsujisawa, S. Kishino, Y.H. Liu, H. Miyake, K. Hiramatsu, T. Shibata, M. Tanaka, Physica Status Solidi (c) **4**, 2252 (2007)
102. A. Koukitu, F. Satoh, T. Yamane, H. Murakami, Y. Kumagai, J. Cryst. Growth **305**, 335 (2007)
103. M. Bickermann, B.M. Epelbaum, A. Winnacker, Physica Status Solidi (c) (2003). https://doi.org/10.1002/pssc.200303280
104. D. Ehrentraut, Z. Sitar, MRS Bull. **34**, 259 (2009)
105. B.M. Epelbaum, M. Bickermann, A. Winnacker, in *Silicon Carbide and Related Materials - 2002*. ed. by P. Bergman, E. Janzen (Trans Tech Publications Ltd, Zurich-Uetikon, 2002), pp. 983–986
106. F.A. Ponce, J.J.S. Major, W.E. Plano, D.F. Welch, Appl. Phys. Lett. **65**, 2302 (1994)
107. H. Amano, M. Iwaya, N. Hayashi, T. Kashima, S. Nitta, C. Wetzel, I. Akasaki, Physica Status Solidi (b) **216**, 683 (1999)
108. O. Yasuo, Y. Hiroaki, S. Rie, Jpn. J. Appl. Phys. **36**, L1565 (1997)
109. H.-M. Wang, J.-P. Zhang, C.-Q. Chen, Q. Fareed, J.-W. Yang, M.A. Khan, Appl. Phys. Lett. **81**, 604 (2002)
110. U. Zeimer, V. Kueller, A. Knauer, A. Mogilatenko, M. Weyers, M. Kneissl, J. Cryst. Growth **377**, 32 (2013)
111. V. Kueller, A. Knauer, F. Brunner, U. Zeimer, H. Rodriguez, M. Kneissl, M. Weyers, J. Cryst. Growth **315**, 200 (2011)
112. J.P. Zhang, H.M. Wang, M.E. Gaevski, C.Q. Chen, Q. Fareed, J.W. Yang, G. Simin, M.A. Khan, Appl. Phys. Lett. **80**, 3542 (2002)
113. W.H. Sun, J.P. Zhang, J.W. Yang, H.P. Maruska, M.A. Khan, R. Liu, F.A. Ponce, Appl. Phys. Lett. **87**, 211915 (2005)
114. H. Fukuyama, H. Miyake, G. Nishio, S. Suzuki, K. Hiramatsu, Jpn. J. Appl. Phys. **55**, 0502 (2016)
115. S. Hagedorn, S. Walde, A. Mogilatenko, M. Weyers, L. Cancellara, M. Albrecht, D. Jaeger, J. Cryst. Growth **512**, 142 (2019)
116. J. Hakamata, Y. Kawase, L. Dong, S. Iwayama, M. Iwaya, T. Takeuchi, S. Kamiyama, H. Miyake, I. Akasaki, Physica Status Solidi (b) **255**, 1700506 (2018)
117. S. Washiyama, Y. Guan, S. Mita, R. Collazo, Z. Sitar, J. Appl. Phys. **127**, 115301 (2020)
118. K. Shojiki, R. Ishii, K. Uesugi, M. Funato, Y. Kawakami, H. Miyake, AIP Adv. **9**, 125342 (2019)
119. J.-M. Bethoux, P. Vennéguès, F. Natali, E. Feltin, O. Tottereau, G. Nataf, P.D. Mierry, F. Semond, J. Appl. Phys. **94**, 6499 (2003)
120. X. Chen, Y. Zhang, J. Yan, Y. Guo, S. Zhang, J. Wang, J. Li, J. Alloys Compd. **723**, 192 (2017)
121. H. Taketomi, Y. Aoki, Y. Takagi, A. Sugiyama, M. Kuwabara, H. Yoshida, Jpn. J. Appl. Phys. **55**, 05FJ05 (2016)
122. R. Molnar, Opt.-Electron. Rev. **10**, 287 (2002)
123. T. Nishida, H. Saito, N. Kobayashi, Appl. Phys. Lett. **79**, 711 (2001)
124. D. Cherns, S.-L. Sahonta, R. Liu, F.A. Ponce, H. Amano, I. Akasaki, Appl. Phys. Lett. **85**, 4923 (2004)
125. L. Hubbard, N. Dietz, M. Vernon, R. Collazo, S. Mita, R. Kirste, Z. Sitar, V.T. Woods, in (SPIE, 2017), p. 11
126. I. Bryan, Z. Bryan, S. Mita, A. Rice, J. Tweedie, R. Collazo, Z. Sitar, J. Cryst. Growth **438**, 81 (2016)
127. I. Bryan, A. Rice, L. Hussey, Z. Bryan, M. Bobea, S. Mita, J. Xie, R. Kirste, R. Collazo, Z. Sitar, Appl. Phys. Lett. **102**, 061602 (2013)
128. R. Dalmau, B. Moody, R. Schlesser, S. Mita, J. Xie, M. Feneberg, B. Neuschl, K. Thonke, R. Collazo, A. Rice, J. Tweedie, Z. Sitar, J. Electrochem. Soc. **158**, H530 (2011)
129. J.R. Grandusky, S.R. Gibb, M.C. Mendrick, L.J. Schowalter, Appl. Phys. Express **3**, 072103 (2010)
130. S. Fritze, A. Dadgar, H. Witte, M. Bügler, A. Rohrbeck, J. Bläsing, A. Hoffmann, A. Krost, Appl. Phys. Lett. **100**, 122104 (2012)
131. K.B. Nam, J. Li, M.L. Nakarmi, J.Y. Lin, H.X. Jiang, Appl. Phys. Lett. **81**, 1038 (2002)
132. J. Xie, S. Mita, L. Hussey, A. Rice, J. Tweedie, J. LeBeau, R. Collazo, Z. Sitar, Appl. Phys. Lett. **99**, 141916 (2011)
133. R. Kirste, M.P. Hoffmann, E. Sachet, M. Bobea, Z. Bryan, I. Bryan, C. Nenstiel, A. Hoffmann, J.-P. Maria, R. Collazo, Z. Sitar, Appl. Phys. Lett. **103**, 242107 (2013)
134. I. Bryan, Z. Bryan, S. Washiyama, P. Reddy, B. Gaddy, B. Sarkar, M.H. Breckenridge, Q. Guo, M. Bobea, J. Tweedie, S. Mita, D. Irving, R. Collazo, Z. Sitar, Appl. Phys. Lett. **112**, 062102 (2018)
135. L. Gordon, J.L. Lyons, A. Janotti, C.G. Van de Walle, Phys. Rev. B **89**, 085204 (2014)
136. M.C. Wagener, G.R. James, F. Omnès, Appl. Phys. Lett. **83**, 4193 (2003)
137. J.S. Harris, J.N. Baker, B.E. Gaddy, I. Bryan, Z. Bryan, K.J. Mirrielees, P. Reddy, R. Collazo, Z. Sitar, D.L. Irving, Appl. Phys. Lett. **112**, 152101 (2018)
138. S. Washiyama, P. Reddy, B. Sarkar, M.H. Breckenridge, Q. Guo, P. Bagheri, A. Klump, R. Kirste, J. Tweedie, S. Mita, Z. Sitar, R. Collazo, J. Appl. Phys. **127**, 105702 (2020)
139. F. Mehnke, X.T. Trinh, H. Pingel, T. Wernicke, E. Janzén, N.T. Son, M. Kneissl, J. Appl. Phys. **120**, 145702 (2016)
140. B. Borisov, V. Kuryatkov, Y. Kudryavtsev, R. Asomoza, S. Nikishin, D.Y. Song, M. Holtz, H. Temkin, Appl. Phys. Lett. **87**, 132106 (2005)
141. S. Li, M.E. Ware, V.P. Kunets, M. Hawkridge, P. Minor, J. Wu, G.J. Salamo, Phys. Status Solidi C **8**, 2182 (2011)
142. O. Ambacher, J. Smart, J.R. Shealy, N.G. Weimann, K. Chu, M. Murphy, W.J. Schaff, L.F. Eastman, R. Dimitrov, L. Wittmer, M. Stutzmann, W. Rieger, and J. Hilsenbeck, *Two-Dimensional Electron Gases Induced by Spontaneous and Piezoelectric*

Polarization Charges in N- and Ga-Face AlGaN/GaN Heterostructures (AIP, 1999)
143. S. Li, M. Ware, J. Wu, P. Minor, Z. Wang, Z. Wu, Y. Jiang, G.J. Salamo, Appl. Phys. Lett. **101**, 122103 (2012)
144. Y.A. Xi, K.X. Chen, F. Mont, J.K. Kim, E.F. Schubert, W. Liu, X. Li, J.A. Smart, J. Cryst. Growth **299**, 59 (2007)
145. L. Eckey, U. Von Gfug, J. Holst, A. Hoffmann, B. Schineller, K. Heime, M. Heuken, O. Schön, R. Beccard, J. Cryst. Growth **189–190**, 523 (1998)
146. J.L. Lyons, A. Janotti, C.G. Vande Walle, Phys. Rev. Lett. **108**, 156403 (2012)
147. H. Amano, M. Kito, K. Hiramatsu, I. Akasaki, Jpn. J. Appl. Phys. **28**, L2112 (1989)
148. Z. Bryan, M. Hoffmann, J. Tweedie, R. Kirste, G. Callsen, I. Bryan, A. Rice, M. Bobea, S. Mita, J. Xie, Z. Sitar, R. Collazo, J. Electron. Mater. **42**, 815 (2013)
149. Y. Arakawa, K. Ueno, A. Kobayashi, J. Ohta, H. Fujioka, APL Mater. **4**, 086103 (2016)
150. W. Kim, A. Salvador, A.E. Botchkarev, O. Aktas, S.N. Mohammad, H. Morcoç, Appl. Phys. Lett. **69**, 559 (1996)
151. J.M. Myoung, K.H. Shim, O. Gluschenkov, C. Kim, K. Kim, S. Kim, S.G. Bishop, J. Cryst. Growth **182**, 241 (1997)
152. A. Klump, M.P. Hoffmann, F. Kaess, J. Tweedie, P. Reddy, R. Kirste, Z. Sitar, R. Collazo, J. Appl. Phys. **127**, 045702 (2020)
153. R. Kirste, M.P. Hoffmann, J. Tweedie, Z. Bryan, G. Callsen, T. Kure, C. Nenstiel, M.R. Wagner, R. Collazo, A. Hoffmann, Z. Sitar, J. Appl. Phys. **113**, 103504 (2013)
154. M. Suzuki, J. Nishio, M. Onomura, C. Hongo, J. Cryst. Growth **189–190**, 511 (1998)
155. J. Li, T.N. Oder, M.L. Nakarmi, J.Y. Lin, H.X. Jiang, Appl. Phys. Lett. **80**, 1210 (2002)
156. Y. Aoyagi, M. Takeuchi, S. Iwai, H. Hirayama, AIP Adv. **2**, 012177 (2012)
157. A.T. Connie, S. Zhao, S.M.D. Sadaf, I. Shih, Z. Mi, X. Du, J. Lin, H. Jiang, Appl. Phys. Lett. **106**, 213105 (2015)
158. X. Wang, W. Wang, J. Wang, H. Wu, C. Liu, Sci. Rep. **7**, 44223 (2017)
159. S.A. Nikishin, V.V. Kuryatkov, A. Chandolu, B.A. Borisov, G.D. Kipshidze, I. Ahmad, M. Holtz, H. Temkin, Jpn. J. Appl. Phys. **42**, L1362 (2003)
160. A.A. Allerman, M.H. Crawford, M.A. Miller, S.R. Lee, J. Cryst. Growth **312**, 756 (2010)
161. C.E. Dreyer, A. Janotti, C.G. Van de Walle, D. Vanderbilt, Phys. Rev. **6**, 021038 (2016)
162. R. Chaudhuri, S.J. Bader, Z. Chen, D.A. Muller, H.G. Xing, D. Jena, Science **365**, 1454 (2019)
163. S. Nakamura, T. Mukai, M. Senoh, Jpn. J. Appl. Phys. **31**, 2883 (1992)
164. G. Greco, F. Iucolano, F. Roccaforte, Appl. Surf. Sci. **383**, 324 (2016)
165. S.K. Kim, J.C. Han, T.-Y. Seong, Jpn. J. Appl. Phys. **55**, 031001 (2016)
166. Z. Fan, S.N. Mohammad, W. Kim, Ö. Aktas, A.E. Botchkarev, H. Morkoç, Appl. Phys. Lett. **68**, 1672 (1996)
167. B. Sarkar, B.B. Haidet, P. Reddy, R. Kirste, R. Collazo, Z. Sitar, Appl. Phys. Express **10**, 071001 (2017)
168. R. France, T. Xu, P. Chen, R. Chandrasekaran, T.D. Moustakas, Appl. Phys. Lett. **90**, 062115 (2007)
169. E.A. Douglas, S. Reza, C. Sanchez, D. Koleske, A. Allerman, B. Klein, A.M. Armstrong, R.J. Kaplar, A.G. Baca, Phys. Status Solidi A **214**, 1600842 (2017)
170. N. Miura, T. Oishi, T. Nanjo, M. Suita, Y. Abe, T. Ozeki, H. Ishikawa, T. Egawa, IEEE Trans. Electron. Dev. **51**, 297 (2004)
171. B.B. Haidet, I. Bryan, P. Reddy, Z. Bryan, R. Collazo, Z. Sitar, J. Appl. Phys. **117**, 245702 (2015)
172. M. Kneissl, in *III-Nitride Ultraviolet Emitters*. ed. by M. Kneissl, J. Rass (Springer, New York, 2016), pp. 1–25
173. J. Chen, W.D. Brewer, Adv. Electron. Mater. **1**, 1500113 (2015)
174. L. Lymperakis, P.H. Weidlich, H. Eisele, M. Schnedler, J.P. Nys, B. Grandidier, D. Stiévenard, R.E. Dunin-Borkowski, J. Neugebauer, P. Ebert, Appl. Phys. Lett. **103**, 152101 (2013)
175. C.G.V. de Walle, J. Neugebauer, J. Appl. Phys. **95**, 3851 (2004)
176. P.-S. Chen, C.-S. Lee, J.-T. Yan, C.-T. Lee, Electrochem. Solid-State Lett. **10**, H165 (2007)
177. B. Sarkar, P. Reddy, A. Klump, F. Kaess, R. Rounds, R. Kirste, S. Mita, E. Kohn, R. Collazo, Z. Sitar, J. Electron. Mater. **47**, 305 (2018)
178. J.-K. Ho, C.-S. Jong, C.C. Chiu, C.-N. Huang, K.-K. Shih, L.-C. Chen, F.-R. Chen, J.-J. Kai, J. Appl. Phys. **86**, 4491 (1999)
179. D. Qiao, L.S. Yu, S.S. Lau, J.Y. Lin, H.X. Jiang, T.E. Haynes, J. Appl. Phys. **88**, 4196 (2000)
180. H. Hirayama, Y. Tsukada, T. Maeda, N. Kamata, Appl. Phys. Express **3**, 031002 (2010)
181. J. Liday, I. Hotový, H. Sitter, P. Vogrinčič, A. Vincze, I. Vávra, A. Šatka, G. Ecke, A. Bonanni, J. Breza, C. Simbrunner, B. Plochberger, J. Mater. Sci.: Mater. Electron. **19**, 855 (2007)
182. H. Omiya, F.A. Ponce, H. Marui, S. Tanaka, T. Mukai, Appl. Phys. Lett. **85**, 6143 (2004)
183. L.-C. Chen, F.-R. Chen, J.-J. Kai, L. Chang, J.-K. Ho, C.-S. Jong, C.C. Chiu, C.-N. Huang, C.-Y. Chen, K.-K. Shih, J. Appl. Phys. **86**, 3826 (1999)
184. N. Braslau, J. Vac. Sci. Technol. **19**, 803 (1981)
185. F. Liang, D. Zhao, D. Jiang, Z. Liu, J. Zhu, P. Chen, J. Yang, W. Liu, X. Li, S. Liu, Y. Xing, L. Zhang, H. Yang, H. Long, M. Li, J. Cryst. Growth **467**, 1 (2017)
186. C.-W. Liao, Y.-H. Lin, C.-Y. Yen, P.-W. Liu, Y.-C. Lu, R.-M. Lin, in *2007 International Semiconductor Device Research Symposium* (2007), pp. 1–2
187. F. Akyol, S. Krishnamoorthy, Y. Zhang, J. Johnson, J. Hwang, S. Rajan, Appl. Phys. Lett. **108**, 131103 (2016)

188. J.T. Leonard, E.C. Young, B.P. Yonkee, D.A. Cohen, T. Margalith, S.P. DenBaars, J.S. Speck, S. Nakamura, Appl. Phys. Lett. **107**, 091105 (2015)
189. S. Krishnamoorthy, F. Akyol, S. Rajan, Appl. Phys. Lett. **105**, 141104 (2014)
190. Y. Ohba, A. Hatano, J. Cryst. Growth **145**, 214 (1994)
191. H. Xing, D.S. Green, H. Yu, T. Mates, P. Kozodoy, S. Keller, S.P. DenBaars, U.K. Mishra, Jpn. J. Appl. Phys. **42**, 50 (2003)
192. A. Agarwal, M. Tahhan, T. Mates, S. Keller, U. Mishra, J. Appl. Phys. **121**, 025106 (2017)
193. Y. Zhang, S. Krishnamoorthy, F. Akyol, A.A. Allerman, M.W. Moseley, A.M. Armstrong, S. Rajan, Appl. Phys. Lett. **109**, 121102 (2016)
194. H. Yoshida, Y. Yamashita, M. Kuwabara, H. Kan, Nat. Photon. **2**, 551 (2008)
195. J.R. Chen, T.S. Ko, P.Y. Su, T.C. Lu, H.C. Kuo, Y.K. Kuo, S.C. Wang, J. Lightwave Technol. **26**, 3155 (2008)
196. K. Kazunobu, F. Kentaro, Y. Yoshiki, M. Hideto, H. Kazumasa, F.C. Shigefusa, Appl. Phys. Express **10**, 015802 (2017)
197. J. Piprek, *Nitride Semiconductor Devices: Principles and Simulation* (Wiley, Hoboken, 2007)
198. M.M. Satter, H.J. Kim, Z. Lochner, J.H. Ryou, S.C. Shen, R.D. Dupuis, P.D. Yoder, IEEE J. Quantum Electron. **48**, 703 (2012)
199. J. Xie, S. Mita, Z. Bryan, W. Guo, L. Hussey, B. Moody, R. Schlesser, R. Kirste, M. Gerhold, R. Collazo, Z. Sitar, Appl. Phys. Lett. **102**, 171102 (2013)
200. L. Coldren, *Diode Lasers and Photonic Integrated Circuits* (Wiley, Hoboken, 2012), pp. 565–577
201. M. Grzegorz, T. Henryk, S. Marcin, W. Pawel, G. Szymon, G. Ewa, P. Piotr, S. Czeslaw, Appl. Phys. Express **8**, 032103 (2015)
202. F. Nippert, M.T. Mazraehno, M.J. Davies, M.P. Hoffmann, H.-J. Lugauer, T. Kure, M. Kneissl, A. Hoffmann, M.R. Wagner, Appl. Phys. Lett. **113**, 071107 (2018)
203. Q. Guo, R. Kirste, S. Mita, J. Tweedie, P. Reddy, S. Washiyama, M.H. Breckenridge, R. Collazo, Z. Sitar, Jpn. J. Appl. Phys. **58**, 10 (2019)
204. Y. Liao, C. Thomidis, C. Kao, T.D. Moustakas, Appl. Phys. Lett. **98**, 081110 (2011)
205. A. Bhattacharyya, T.D. Moustakas, L. Zhou, D.J. Smith, W. Hug, Appl. Phys. Lett. **94**, 181907 (2009)
206. W. Guo, Z. Bryan, J.Q. Xie, R. Kirste, S. Mita, I. Bryan, L. Hussey, M. Bobea, B. Haidet, M. Gerhold, R. Collazo, Z. Sitar, J. Appl. Phys. **115**, 103108 (2014)
207. E.F. Pecora, W. Zhang, AYu. Nikiforov, J. Yin, R. Paiella, L.D. Negro, T.D. Moustakas, J. Appl. Phys. **113**, 013106 (2013)
208. B. Witzigmann, F. Römer, M. Martens, C. Kuhn, T. Wernicke, M. Kneissl, AIP Adv. **10**, 095307 (2020)
209. J.W. Ferguson, P. Blood, P.M. Smowton, H. Bae, T. Sarmiento, J.S. Harris, N. Tansu, L.J. Mawst, in (2011), pp. 1–2.
210. A. Thränhardt, I. Kuznetsova, C. Schlichenmaier, S.W. Koch, L. Shterengas, G. Belenky, J.-Y. Yeh, L.J. Mawst, N. Tansu, J. Hader, J.V. Moloney, W.W. Chow, Appl. Phys. Lett. **86**, 201117 (2005)
211. W.W. Chow, M. Kneissl, J. Appl. Phys. **98**, 114502 (2005)
212. Y.P. Gong, K. Xing, T. Wang, Appl. Phys. Lett. **99**, 171912 (2011)
213. T. Deguchi, T. Azuhata, T. Sota, S. Chichibu, S. Nakamura, Mater. Sci. Eng. B **50**, 251 (1997)
214. H. Murotani, R. Tanabe, K. Hisanaga, A. Hamada, K. Beppu, N. Maeda, M.A. Khan, M. Jo, H. Hirayama, Y. Yamada, Appl. Phys. Lett. **117**, 162106 (2020)
215. M.E. Levinshteĭn, S.L. Rumyantsev, M. Shur, *Properties of Advanced Semiconductor Materials GaN AlN InN, BN, SiC, SiGe* (John Wiley, New York, 2001)
216. G. Muziol, H. Turski, M. Siekacz, S. Grzanka, P. Perlin, C. Skierbiszewski, Appl. Phys. Express **9**, 092103 (2016)
217. H. Yang, D. Zhao, S.-C. Liu, Y. Liu, J.-H. Seo, M. Hodek, Z. Ma, J.D. Albrecht, B. Moody, W. Zhou, in *Conference on Lasers and Electro-Optics (2016), Paper STu3R.3* (Optical Society of America, 2016), p. STu3R.3
218. T.-T. Kao, Y.-S. Liu, M.M. Satter, X.-H. Li, Z. Lochner, P. Douglas Yoder, T. Detchprohm, R.D. Dupuis, S.-C. Shen, J.-H. Ryou, A.M. Fischer, Y. Wei, H. Xie, F.A. Ponce, Appl. Phys. Lett. **103**, 211103 (2013)
219. T. Sakai, M. Kushimoto, Z. Zhang, N. Sugiyama, L.J. Schowalter, Y. Honda, C. Sasaoka, H. Amano, Appl. Phys. Lett. **116**, 122101 (2020)
220. M.H. Crawford, A.A. Allerman, A.M. Armstrong, M.L. Smith, K.C. Cross, Appl. Phys. Express **8**, 112702 (2015)
221. K. Iida, T. Kawashima, A. Miyazaki, H. Kasugai, S. Mishima, A. Honshio, Y. Miyake, M. Iwaya, S. Kamiyama, H. Amano, I. Akasaki, Jpn. J. Appl. Phys. **43**, L499 (2004)
222. S. Kamiyama, K. Iida, T. Kawashima, H. Kasugai, S. Mishima, A. Honshio, Y. Miyake, M. Iwaya, H. Amano, I. Akasaki, IEEE J. Sel. Top. Quantum Electron. **11**, 1069 (2005)
223. K. Hiramatsu, J. Phys. Condens. Matter **13**, 6961 (2001)
224. K. Hiramatsu, K. Nishiyama, M. Onishi, H. Mizutani, M. Narukawa, A. Motogaito, H. Miyake, Y. Iyechika, T. Maeda, J. Cryst. Growth **221**, 316 (2000)
225. M. Kuwabara, Y. Yamashita, K. Torii, H. Yoshida, Jpn. J. Appl. Phys. **52**, 08JG10 (2013)
226. B.H. Le, X. Liu, N.H. Tran, S. Zhao, Z. Mi, Opt. Express **27**, 5843 (2019)
227. K. Sato, S. Yasue, K. Yamada, S. Tanaka, T. Omori, S. Ishizuka, S. Teramura, Y. Ogino, S. Iwayama, H. Miyake, M. Iwaya, T. Takeuchi, S. Kamiyama, I. Akasaki, Appl. Phys. Express **13**, 031004 (2020)
228. M. Shatalov, M. Gaevski, V. Adivarahan, A. Khan, Jpn. J. Appl. Phys. **45**, L1286 (2006)

229. H. Amano, N. Watanabe, N. Koide, I. Akasaki, Jpn. J. Appl. Phys. **32**, L1000 (1993)
230. T.J. Schmidt, X.H. Yang, W. Shan, J.J. Song, A. Salvador, W. Kim, Ö. Aktas, A. Botchkarev, H. Morkoç, Appl. Phys. Lett. **68**, 1820 (1996)
231. T. Takano, Y. Narita, A. Horiuchi, H. Kawanishi, Appl. Phys. Lett. **84**, 3567 (2004)
232. M. Kneissl, Z. Yang, M. Teepe, C. Knollenberg, O. Schmidt, P. Kiesel, N.M. Johnson, S. Schujman, L.J. Schowalter, J. Appl. Phys. **101**, 123103 (2007)
233. X.-H. Li, T. Detchprohm, T.-T. Kao, M.D.M. Satter, S.-C. Shen, P.D. Yoder, R.D. Dupuis, S. Wang, Y.O. Wei, H. Xie, A.M. Fischer, F.A. Ponce, T. Wernicke, C. Reich, M. Martens, M. Kneissl, Appl. Phys. Lett. **105**, 141106 (2014)
234. Y. Tian, J. Yan, Y. Zhang, X. Chen, Y. Guo, P. Cong, L. Sun, Q. Wang, E. Guo, X. Wei, J. Wang, J. Li, Opt. Express **23**, 11334 (2015)
235. T. Wunderer, C.L. Chua, J.E. Northrup, Z. Yang, N.M. Johnson, M. Kneissl, G.A. Garrett, H. Shen, M. Wraback, B. Moody, H.S. Craft, R. Schlesser, R.F. Dalmau, Z. Sitar, Physica Status Solidi (c) **9**, 822 (2012)